

## AVERAGE PROPERTIES OF A LARGE SAMPLE OF $z_{\text{abs}} \sim z_{\text{em}}$ ASSOCIATED Mg II ABSORPTION LINE SYSTEMS

DANIEL VANDEN BERK

Department of Astronomy and Astrophysics, The Pennsylvania State University, 525 Davey Laboratory, University Park, PA 16802

PUSHPA KHARE

Department of Physics, Utkal University, Bhubaneswar, 751004, India

DONALD G. YORK<sup>1</sup>

Department of Astronomy and Astrophysics, University of Chicago, Chicago, IL 60637

GORDON T. RICHARDS<sup>2</sup>

Department of Physics, Drexel University, 3141 Chestnut Street, Philadelphia, PA 19104

BRITT LUNDGREN

Department of Astronomy, University of Illinois at Urbana-Champaign, MC-221 1002 West Green Street, Urbana, IL 61801

YUSRA ALSAYYAD

Department of Astronomy and Astrophysics, University of Chicago, Chicago, IL 60637

VARSHA P. KULKARNI

Department of Physics and Astronomy, University of South Carolina, Columbia, SC 29207

MARK SUBBARAO<sup>3</sup>

Department of Astronomy and Astrophysics, University of Chicago, Chicago, IL 60637

DONALD P. SCHNEIDER

Department of Astronomy and Astrophysics, The Pennsylvania State University, 525 Davey Laboratory, University Park, PA 16802

TIM HECKMAN

Department of Physics and Astronomy, Homewood Campus, Baltimore, MD 21218

SCOTT ANDERSON

Department of Astronomy, University of Washington, Box 351580, Seattle, WA 98195

ARLIN P. S. CROTTIS

Department of Astronomy, Columbia University, New York, NY 10027

JOSH FRIEMAN AND C. STOUGHTON

Fermilab National Accelerator Laboratory, P.O. Box, 500, Batavia, IL, 60510

JAMES T. LAUROESCH

Department of Physics and Astronomy, University of Louisville, Louisville, KY 40292

PATRICK B. HALL

Department of Physics and Astronomy, York University, 4700 Keele Street, Toronto, ON M3J 1P3, Canada

AVERY MEIKSIN

Institute of Astronomy, Royal Observatory, University of Edinburgh, Blackford Hill, Edinburgh, EH9 3HJ, UK

AND

MICHAEL STEFFING AND JOHNNY VANLANDINGHAM

Department of Astronomy and Astrophysics, University of Chicago, Chicago, IL 60637

*Received 2007 July 3; accepted 2008 January 23*

### ABSTRACT

We studied a sample of 415 associated ( $z_{\text{abs}} \sim z_{\text{em}}$ ; relative velocity with respect to QSO in units of  $c$ ,  $\beta < 0.01$ ) Mg II absorption systems with  $1.0 \leq z_{\text{abs}} \leq 1.86$ , in the spectra of SDSS DR3 QSOs, to determine the dust content and ionization state in the absorbers. We also compared these properties to those of a similarly selected sample of 809 intervening systems ( $\beta > 0.01$ ), so as to understand their origin. Normalized, composite spectra were derived for absorption line measurements, for the full sample and for several subsamples, chosen on the basis of the line strengths and other absorber and QSO properties. From these, and from the equivalent widths in individual spectra, we conclude that the associated Mg II absorbers have higher ionization (higher ratios of the strengths of C IV and Mg II lines), than the intervening absorbers. The ionization decreases with increasing  $\beta$ . Average extinction curves were obtained for the subsamples by comparing their geometric mean QSO spectra with those of matching (in  $z_{\text{em}}$  and

<sup>1</sup> Also at: Enrico Fermi Institute, University of Chicago, Chicago, IL 60637.

<sup>2</sup> Also at: Department of Physics and Astronomy, The Johns Hopkins University, 3400 North Charles Street, Baltimore, MD 21218.

<sup>3</sup> Also at: Adler Planetarium and Astronomy Museum, 1300 South Lake Shore Drive, Chicago, IL 60605.

*i* magnitude) samples of QSOs without absorption lines. There is clear evidence for SMC-like dust attenuation in these systems; the 2175 Å absorption feature is absent. The extinction is almost twice that observed in intervening systems. We reconfirm that QSOs with nonzero FIRST radio flux are intrinsically redder than the QSOs with no detection in the FIRST survey. The incidence of associated Mg II systems in radio-detected QSOs is 1.7 times that in radio-undetected QSOs. The associated absorbers in radio-detected QSOs cause 3 times more reddening than those in radio-undetected QSOs. This excess reddening is correlated with the strength of Mg II absorption, possibly suggesting an intrinsic nature for the associated absorbers in radio-detected QSOs.

*Subject headings:* dust, extinction — ISM: abundances — quasars: absorption lines

*Online material:* machine-readable tables

## 1. INTRODUCTION

Many of the first detected narrow-line QSO absorption systems had redshifts close to those of their QSOs (e.g., Stockton & Lynds 1966; Burbidge et al. 1966). Such systems, having a relative velocity with respect to the QSO in units of the speed of light,<sup>4</sup>  $\beta$ , smaller than 0.02, are now termed associated systems. Study of the associated systems is important to understand the energetics and kinematics near the central black hole and also for understanding the ionization structure, dust content, and abundances in material directly exposed to radiation from QSOs, and in some cases, possibly ejected from the QSOs or the accretion disks. Associated systems have been suggested to arise (A) in the outer parts of QSO host galaxies (e.g., Heckman et al. 1991; Chelouche et al. 2007), which may have gas properties similar to those in the outer parts of inactive galaxies (Steidel et al. 1997; Fukugita & Peebles 2006); (B) by material within 30 kpc of the active galactic nucleus (AGN), accelerated by starburst shocks from the inner galaxy (e.g., Heckman et al. 1990, 1996; D’Odorico et al. 2004; Fu & Stockton 2007a); or (C) in the core of the AGN, within 10 pc of the black hole (Hamann et al. 1997a, 1997b; Barlow & Sargent 1997).

In case A, these are possibly “halo” clouds as in normal galaxies, possibly lit up by the QSO to produce extended regions of Ly $\alpha$  emission, but not thought to be moving at the high velocities necessary to explain the dispersion of associated system velocities with respect to the QSO itself. However, using spectra of a set of angularly close QSO pairs, Bowen et al. (2006) confirmed that gas in the outer parts of some QSO host galaxies is detectable as absorption in the spectra of background QSOs, but the spectra of the foreground QSOs did not reveal associated absorption systems: evidently, the appearance of the absorption is dependent on the angle of the line of sight to the spin axis of the accretion disk. The low velocities expected from such gas led to the postulate that clusters of galaxies near the QSO showing associated absorption were responsible for the absorption and the dispersion of cloud velocities. However, QSOs are not only associated with clusters of galaxies: they appear in a wide range of galaxy types and masses (Jahnke et al. 2004), and, while found in slightly higher density environments (Serber et al. 2006), do not require cluster type densities on large scales (Wake et al. 2004).

In case B, the gas is typically found to have densities of a few hundred particles cm<sup>-3</sup>, high enough to produce excited fine-structure lines of Si II and C II. There are suggestions in the above references that this is material ejected by a galactic wind, possibly a superwind from a starburst (Heckman et al. 1990), then lit up by the QSO. (These are often called extended emis-

sion line regions, or EELR). Cooling flows (Crawford & Fabian 1989) no longer seem to be considered in most cases (Fu & Stockton 2007b).

In case C, absorption is inferred to be very close to the black hole because of variability in the absorption lines, and/or because of the presence of clouds that do not cover the source. Theoretical investigations of case C (Arav et al. 1994; Konigl & Kartje 1994; Murray et al. 1995; Krolik & Kriss 2001; Proga et al. 2000; Everett 2005; and Chelouche & Netzger 2005, for a Seyfert galaxy with a much lower radiation field), have reinforced the plausibility of thermal or hydromagnetic radiation assisted flows, both parallel to the AGN jet axis and perpendicular to it, along the accretion disk. See, for example, Figure 13 of Konigl & Kartje (1994), Figure 1 of Richards et al. (1999), Figure 1 of Murray et al. (1995), and Figure 1 of Everett (2005).

Early studies concentrated on systems with C IV doublets. Weymann et al. (1979) and Foltz et al. (1986) found a statistical excess of such systems as compared to what was expected if these were randomly distributed in space. Other studies (Young et al. 1982; Sargent et al. 1988) could not confirm these observations. Later it was shown that Mg II systems (Aldcroft et al. 1994) and C IV systems (Anderson et al. 1987; Foltz et al. 1988) with  $\beta < 0.0167$  are preferentially found in steep-spectrum radio sources, often thought of as sources dominated by emission from lobes rather than the core of the source. Ganguly et al. (2001) showed that high-ionization systems (having lines of C IV, N V, and O VI) with  $\beta < 0.0167$  and  $z_{\text{abs}} < 1.0$  are not present in radio-loud QSOs that have compact radio morphologies, flat radio spectra (core-dominated sources), and C IV lines with mediocre FWHM ( $\leq 6000$  km s<sup>-1</sup>). Baker et al. (2002), from a study of a near-complete sample of low-frequency-selected, radio-loud QSOs, corroborated trends for C IV-associated absorption to be found preferentially in steep-spectrum and lobe-dominated QSOs, suggesting that the absorption is the result of poststarburst activity and that the C IV lines weaken as the radio source grows, clearing out the gas and dust. Vestergaard (2003, hereafter V03) studied a sample of high-ionization associated systems with  $1.5 < z_{\text{abs}} < 3.5$  and found that the occurrence, or not, of such systems is independent of radio properties of the QSOs. V03 did not find the relationship between radio source size and C IV line strength of Baker et al. (2002), nor the absence of absorbers in low linewidth systems of Ganguly et al. (2001). V03 did identify weak correlations among QSO properties and the line strengths of the associated absorption systems, which differed from those of the intervening systems, but concluded that differences in the results among the three studies (Baker et al. 2002; Vestergaard 2003; Ganguly et al. 2001) could probably be attributed to various differences in selection of the relatively small samples (50–100 systems): among them, the most

<sup>4</sup>  $\beta = [(1 + z_{\text{em}})^2 - (1 + z_{\text{abs}})^2] / [(1 + z_{\text{em}})^2 + (1 + z_{\text{abs}})^2]$ .

obvious difference is the optical luminosity of the samples, progressively more luminous in order of the references just cited.

Steep-spectrum radio sources, from the above references, have an excess of associated ( $\beta < 0.02$ ) absorbers and are thought to be viewed at a large angle to the jet axis, so the sight line passes over the accretion disk (or torus). Broad absorption line (BAL) systems are often thought to be viewed from the same aspect, but are generally devoid of radio flux. There are suggestions that the associated systems are related in some way to the broad absorption line systems (Wampler et al. 1995; Baker et al. 2002; V03), summarized by V03.

There have also been suggestions that narrow-line QSO absorption-line systems (QSOALS) that have high velocities with respect to the QSO, i.e., apparent velocities of ejection up to tens of thousands of  $\text{km s}^{-1}$  may also be associated with the QSOs, meaning they are close to the QSO ( $\ll 10$  pc) but have high relative velocity (Vanden Berk et al. 1996; Januzzi et al. 1996; Richards et al. 1999; Richards 2001; V03; Misawa et al. 2007); candidate systems are especially noticeable in the brightest QSOs and in radio sources with flat radio spectra (often said to be core-dominated sources). Richards et al. (2001), using the largest sample of radio QSOs available to date, showed that there is an excess of C IV absorbers at high  $\beta$  values in flat-spectrum radio sources (thought to be viewed close to the jet axis), strengthening arguments of Richards et al. (1999) and Richards (2001) that up to 36% of the apparently high-velocity material is associated with material intrinsic to the background AGN. As shown by Misawa et al. (2007), such material may evidently reach very high outflow velocities, up to and exceeding  $20,000 \text{ km s}^{-1}$ . Their evidence for the intrinsic nature of such components is the small filling factor of the absorption lines in covering the background UV radiation source, presumably the full accretion disk (Pereyra et al. 2006). A primary question is how to tell if a given system is intrinsic or not, whatever its  $\beta$  value.

In this paper, we use a large and homogeneous sample of associated ( $z_{\text{abs}} \sim z_{\text{em}}$ ; relative velocity with respect to the QSO  $< 3000 \text{ km s}^{-1}$ ) Mg II systems with  $1.0 < z_{\text{abs}} < 1.86$  compiled from the Sloan Digital Sky Survey (SDSS) Data Release 3 (DR3) catalog to determine the average dust content, ionization, and relative abundances in these absorbers. Our aim is to determine if these systems are indeed intrinsic to the QSOs by (1) studying the dependence of their average properties on QSO properties and (2) comparing the properties of associated Mg II systems with those of intervening systems ( $\beta > 0.01$ ) selected with similar criteria. In particular, we are looking for a spectroscopic signature to distinguish associated from intervening systems.

We make use of the composite spectra of the sample (and various subsamples thereof), following the method recently advocated by York et al. (2006, hereafter Y06). In § 2 we describe the criteria used for sample selection, various subsamples generated from the main sample, and the method of generating composite spectra. In § 3 we present our results which include (1) a comparison between the properties of the samples of the intervening and associated systems, using several statistical tests; (2) a discussion of the line strengths in the composite spectra of associated systems compared to those for the intervening sample and of the state of ionization in these systems; (3) the measured extinction for various subsamples; (4) a detailed analysis of the dependence of extinction and other properties on the radio properties of the QSOs; (5) a discussion of the abundances in associated sample; and (6) possible scenarios for the origin and location of the absorbers. A few systematic effects that may be hidden in our data are noted in § 4. Conclusions are presented in § 5.

## 2. ANALYSIS

### 2.1. Sample Selection

The absorption-line system sample used here was selected from the SDSS DR3 absorption-line catalog compiled by York et al. (2005, 2006). In this section we describe the SDSS, the QSO sample in which the absorbers are discovered, the construction of the SDSS absorber catalog, and finally the selection of the associated absorption-line systems used in this study.

The SDSS (York et al. 2000; Stoughton et al. 2002) is an imaging and spectroscopic survey carried out from Apache Point Observatory, near Sunspot, New Mexico, using a 2.5 m telescope (Gunn et al. 2006). Candidate QSOs are color-selected from five-color scans with a CCD camera (Gunn et al. 1998) of the 10,000 square degrees of the sky north of Galactic latitude  $30^\circ$ . The photometry from that imaging survey is based on a specially constructed set of filters (Fukugita et al. 1996), calibrated with tertiary standards in the imaging scans (Tucker et al. 2006). The establishment of secondary standards using the SDSS Photometric Telescope (Hogg et al. 2001) and the 1 m telescope at the US Naval Observatory (Flagstaff), and their tie to a primary standard, is described by Ivezić et al. (2004) and Smith et al. (2002). The photometry is better than  $\pm 0.02$  mag in all bands (Adelman-McCarthy et al. 2007).

The QSOs are color selected (Richards et al. 2002a) from the reduced, archived photometric data. Spectra are obtained using two dual spectrographs. Plates are drilled with 640  $3''$  diameter holes, distributed over an area of  $7 \text{ deg}^2$ , into which optical fibers are inserted by hand. About 100 of the fibers are allocated to QSOs. The selection of QSOs is meant to be complete to magnitude 19.1 in the SDSS  $i$  band, except that two objects within  $55''$  of each other cannot be observed using the same plate; one QSO must sometimes be picked over another, or a galaxy may take higher priority over a nearby QSO in the plate planning process. (Multiple adjacent QSOs exist in the archive because a second plate can be planned to overlap with a previous plate; Blanton et al. 2003.) The astrometry, accurate to  $< 0.1''$ , which allows precise placement of the fibers is described by Pier et al. (2003). The plates are manually plugged and are used on nights not normally acceptable for imaging. Typically 45 to 60 minutes of exposure are obtained in several 15 minute integrations, when cloudless skies prevail. The exposure times or the total number of exposures are adjusted so the end result yields  $(S/N)^2 \sim 7$  for an object of  $g$  magnitude 20.1. The selection of objects yields a set of QSO spectra with about 70% efficiency (some selected objects are not QSOs), complete to better than 90% (Vanden Berk et al. 2005). Each plate includes fibers allocated to standard stars for flux calibration and for sky removal. Below  $i = 19.1$ , QSOs are also included in the selection if they are X-ray sources from *ROSAT* (Voges et al. 1999) or radio sources from the VLA FIRST (Faint Images of the Radio Sky at Twenty cm) survey (Becker et al. 1995).

These spectra are reduced with two pipelines (two-dimensional extraction and one-dimensional analysis). The QSO emission redshift is determined by the SDSS pipeline, first assembling a list of emission peaks using a wavelet based, peak-finding algorithm. These are matched against a standard set of strong QSO emission lines to find the best-fit redshift (SubbaRao et al. 2002).

The assembly of the archive of all QSOALSs in the spectra occurs in a separate pipeline (York et al. 2005), run after the authoritative QSO spectra are prepared for publication (Schneider et al. 2005 for DR3; Schneider et al. 2007 for DR5). A more complete description of the pipeline is in preparation (York et al., in preparation). Briefly, significant (equivalent width  $> 3 \sigma$ ,  $\sigma$

being the uncertainty in the equivalent width measurement due to noise in the spectrum; for narrow-line QSOALS, the continuum error is smaller, in general, than the error due to noise), narrow (typically 3–8 pixels, each  $70 \text{ km s}^{-1}$  in width) absorption features are identified after fitting a smooth continuum to the spectrum. Poor night sky subtraction is easily recognized, and features found do not include such artifacts. BALs are identified and flagged separately (Trump et al. 2006 for DR3, the data release used in this paper); no lines are picked for this study from QSOs that contain known BALs. However, most BALs in the SDSS are detected by the presence of C IV absorption, and only a small fraction have detectable Mg II absorption (e.g., Trump et al. 2006). About half of the QSOs in our sample of associated absorbers (described below) have  $z_{\text{em}} < 1.5$  and cannot be determined to be free of BAL systems, since C IV emission is not redshifted into the SDSS spectra until  $z_{\text{em}} \geq 1.5$ . A search is first done for C IV doublets (one line is picked and other line with the correct separation in wavelength is searched for), then for Mg II doublets, then for various Fe II pairs of lines (in case one line of Mg II is exactly at one of a select set of night sky lines, or is obliterated by a poor correction for other lines).

Other lines are then selected by their correspondence to the Mg II, Fe II, or C IV candidate systems. Unidentified lines are cataloged. These catalogs have been carefully checked by hand to verify that our selection is not missing some extreme situations that are not “normal” but would be extremely interesting if real.<sup>5</sup> Thousands of systems have been examined, and the rules above are secure. Among lines identified as being within a line width of the main lines noted above, those that are significant at the  $4 \sigma$  level, those identified as being unambiguous (i.e., not possibly blended with a line from another absorption line system), and those not in the Ly $\alpha$  forest of that QSO are selected to provide a quality grade for each system. Four such selected lines produces a grade A system; three lines a grade B system; and two lines a grade C system. Systems with only one line above a  $4 \sigma$  significance, and those with lines that are all detected with a significance between 3 and  $4 \sigma$ , are, respectively, considered for classification as grade D or E systems. The lines used for grading are primary lines usually seen in QSO absorption-line systems; not all detected lines are used, even if they fit all the other requirements. For instance, Fe I is not used, because any time that line would be seen, Fe II would be present and stronger. This set of rules is constantly checked by eye, again, so as not to miss recognition of potentially interesting systems. The lines used for grading are the strongest lines of Mg I, C II, Mg II, Al II, Fe II, Al III, C IV and Si IV. Under this set of protocols, for instance, C IV-only systems would be given grades of C, while systems with significant C IV lines accompanied by a line of Si IV or Mg II would be given grades of B, at least. If multiple Si IV and/or Mg II, or gradeable lines of other species are present in the systems, the grades would be A.

The catalog thus constructed can be subjected to an SQL search that produces the sample of systems that one is interested in. For this study, we selected grade A systems, containing Mg II lines with the stronger member of the doublet having  $W_{\text{Mg II}} > 0.3 \text{ \AA}$  that are not in BAL QSOs, have absorber redshifts  $1.0 \leq z_{\text{abs}} \leq 1.86$ , have  $\beta < 0.01$ , and are in QSOs that have

$z_{\text{em}} < 1.96$ . Each system was verified by visual inspection, and any BALs present were eliminated. These systems form our main sample (sample 1), consisting of 415 systems. The list of QSOs in this sample, along with their properties [ $z_{\text{em}}$ ,  $z_{\text{abs}}$ ,  $\beta$ ,  $i$  magnitude, and  $\Delta(g - i)$ <sup>6</sup>] are given in Table 5 in the Appendix. The absorber rest-frame equivalent widths of the prominent lines, along with  $1 \sigma$  errors, are given in Table 6 of the Appendix. About 100 of these do have additional grade A and B systems (at absorption redshifts  $\ll z_{\text{em}}$ ) in their spectra. In principle, these can contribute to the reddening of the parent QSO spectrum, but we show in the next section that they do not contribute to the extinction. Lines in those systems do not contribute to our composite spectrum used for measuring absorption lines, because they are masked before averaging the spectra.

The reasons for the particular selection of systems described above are as follows. It is generally believed (e.g., Rao & Turnshek 2000; Churchill et al. 1999) that systems with  $W_{\text{Mg II}} > 0.3 \text{ \AA}$  have  $N_{\text{H I}} > 3 \times 10^{17} \text{ cm}^{-2}$ . Thus, the Mg II line strengths were restricted so as to choose systems that might have sufficiently large column densities in H I to have significant dust columns. The redshift range of the absorbers was chosen to allow, on the one hand, only objects for which the 2175  $\text{\AA}$  feature lies completely within the SDSS spectrograph wavelength range, and, on the other hand, to ensure that the Mg II lines are at  $\lambda < 8000 \text{ \AA}$ , to avoid the regions of the SDSS spectra that are contaminated by strong night sky emission lines. The restriction on  $z_{\text{em}}$  was imposed to keep the Ly $\alpha$  forest out of the SDSS spectra. We use the range  $\beta < 0.01$  to get the purest sample of associated systems possible, on the presumption that the higher the  $\beta$ , the more likely there are intervening systems mixed in.

We wish to emphasize that the selection criteria were taken to be same as those used by Y06 (except for the range of  $\beta$  values). This was done so that we can compare the properties of the intervening systems (studied by Y06) with those of associated systems (systems with  $z_{\text{abs}} \simeq z_{\text{em}}$ , studied here) without any selection bias. Such a comparison may indicate some signatures that may point toward the latter systems being intrinsic to the QSOs. Our use of class A systems precludes including C IV-only or Mg II-only systems, and we plan to study those systems in a later paper.

Having made the choice to study Mg II associated systems, since we already have a comparison sample of intervening systems, we nevertheless find that our selection is typical, despite the preference of previous authors to focus mainly on systems with C IV and higher ions. First, examination of the complete set of systems selected (Tables 5 and 6) reveals that 89% have significant C IV lines, when those lines are observable in SDSS spectra. Second, a preliminary study of the statistics of all class A and B absorption line systems as a function of  $\beta$  (avoiding systems in BAL QSOs) revealed that the peak in the number distribution of C IV systems for  $-0.003 < \beta < 0.01$  is mimicked when Mg II systems are used (without reference to whether they have C IV or not) These statistics will be the subject of a future paper (D. Vanden Berk et al., in preparation).

A remark is in order about the values of  $\beta$  derived. Gaskell (1982) and Wilkes (1984) showed that the redshifts of QSOs differ from line to line. As summarized by Richards et al. (2002b), the [O III] redshifts generally agree with the stellar absorption line

<sup>5</sup> An example of a new type of system is given by D’Odorico (2007). The lines of neutral Si I, Fe I, and Ca I are seen for the first time in a QSOALS. Our rules would still find this system, although the relatively weak lines of Fe II and Mg II and the even weaker lines of the noted neutral species would only be visible in a few SDSS spectra with extremely high S/N.

<sup>6</sup> This is defined as the difference between the  $(g - i)$  color of a QSO and the median value of  $(g - i)$  of all other verified SDSS QSOs with nearly the same redshift (Richards et al. 2003), and it complements our use of the extinction curves to derive  $E(B - V)$  [ $E(B - V) \sim \Delta(g - i)/4$ ; Y06].

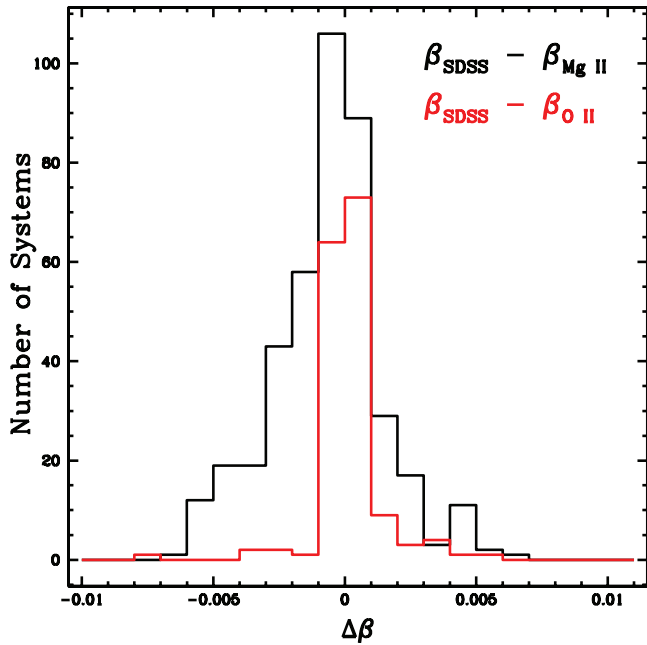


FIG. 1.— Difference between the  $\beta$  values derived for the Mg II associated absorption systems using SDSS redshifts ( $\beta_{\text{SDSS}}$ ) and the single line [O II] ( $\beta_{\text{O II}}$ ; red) or the single line Mg II redshifts ( $\beta_{\text{Mg II}}$ ; black). [O II] is available for 162 QSOs, Mg II is available for 415 QSOs. The single-line [O II] and Mg II emission-line redshifts are derived from the SDSS pipeline. The [O II] line is regarded as giving the best systemic redshift when it is available. The  $\beta$  [O II] values agree very well with the derived SDSS values, which are used in this paper.

redshifts of the host galaxies of the QSOs, when these can be observed. The shifts of Mg II emission compared to the rest-frame narrow emission-line regions defined by [O II] and [O III] is  $<200 \text{ km s}^{-1}$  (Vanden Berk et al. 2001; Tytler & Fan 1992) and probably about  $-100 \text{ km s}^{-1}$  (Richards et al. 2002b). Richards et al. (2002b) and Richards (2006) studied this effect in SDSS QSOs and advocated the removal of the systematic shift, mainly caused by the asymmetric profile of the C IV emission blend, by using the wavelength of  $1546 \text{ \AA}$  instead of the normal  $1549 \text{ \AA}$ . This procedure is adopted in the SDSS pipelines. For 250 QSOs in our sample, the C IV line is available and used in deriving the redshift from the SDSS data, by the SDSS pipeline. The species Mg II and [C III] are available for all spectra. The system redshift reference, [O II], is covered in several spectra, but not always detected. Figure 1 shows the comparison of relative velocities of the absorption systems (with respect to the QSOs), namely  $\beta_{\text{SDSS}}$ ,  $\beta_{\text{[O II]}}$  and  $\beta_{\text{Mg II}}$ , respectively obtained using (1) the SDSS emission redshifts (described above), (2) single-line [O II] redshifts when available (for 162 systems in our sample), and (3) single-line Mg II redshifts (available for all QSOs in our sample, by selection). The single-line [O II] and Mg II redshifts are obtained from the SDSS pipeline. It is apparent that the procedure adopted by the SDSS pipeline does very well in picking the systemic redshifts of the QSOs, and we adopt them in this paper. These redshifts are statistically more precise than the single-line redshifts, which are sometimes based on weak lines. The errors in  $\beta$  are generally  $<500 \text{ km s}^{-1}$ , where we can check directly with [O II]. We therefore feel that the trends we discover later are not caused by errors in the QSO redshifts used here. Letawe et al. (2007), from an analysis of five objects, have shown that the peak of the H $\beta$  line may be a good indicator of systemic redshifts. However, for our sample ( $z_{\text{em}} > 1$ ), the H $\beta$  lines are outside the SDSS spectra, and cannot be used to determine the systemic redshifts.

## 2.2. Generation of Arithmetic Mean and Geometric Mean Composite Spectra

Composite spectra in the absorber rest frame were generated in order to compare continuum and absorption properties of various subsamples of absorption systems. Both arithmetic mean and geometric mean spectra were generated; the arithmetic mean produces a better representation of the average absorption-line profiles, while the geometric mean is better at preserving the continuum properties of the QSOs. The procedure for generating the composites is summarized here, and fully described by Y06.

For the analysis of absorption lines, normalized arithmetic mean spectra were generated as follows. The spectra of individual QSOs were corrected for Galactic reddening (Fitzpatrick 1999; Schlegel et al. 1998) and (along with the associated error arrays) normalized by reconstructions of the QSO continua, using the first 30 QSO eigenspectra derived by Yip et al. (2004). The normalized spectra were shifted to the absorber rest frame and resampled onto a common pixel-to-wavelength scale. Pixels flagged by the spectroscopic pipeline as possibly bad in some way (Stoughton et al. 2002) were masked and not used in constructing the composites. Also masked were the pixels within  $5 \text{ \AA}$  of the expected line positions of detected absorption systems unrelated to the target system. The normalized flux density in each remaining pixel was weighted by the inverse of the associated variance, and the weighted arithmetic mean of all contributing spectra was calculated for each pixel. The number of individual spectra, and the distribution of absorber redshifts, contributing to the composite spectrum of a particular line transition vary from line to line. That is because the absorption system sample was selected to simultaneously cover the Mg II doublet and  $2175 \text{ \AA}$  feature, which means that other transitions may not be covered by all of the spectra. The rest-wavelength range of maximum sensitivity to absorption features in the composite spectra, which gets contributions from all QSOs in the sample, is  $1900\text{--}3150 \text{ \AA}$ ; the rest-frame spectrum of a QSO with absorption system at  $z_{\text{abs}}$  of 1 will cover the range  $1900\text{--}4500 \text{ \AA}$ , while that of a QSO with an absorption system at  $z_{\text{abs}}$  of 1.86 will cover the range  $1330\text{--}3150 \text{ \AA}$ . Thus, the C IV lines are averages of spectra of QSOs with absorption systems with  $z_{\text{abs}} > 1.4765$ , while the Ca II lines are averages of spectra of QSOs with absorption systems with  $z_{\text{abs}} < 1.267$ . Accordingly, the apparent noise in the composite spectra near these lines is greater than that near lines, which fall in the rest-frame  $1900\text{--}3150 \text{ \AA}$  region (which gets contributions from all systems of the sample). Therefore, the mean Ca II line and the mean C IV line cannot be assumed to give an average picture of the relative behavior of the two lines. A subsample must be confined to appropriate  $z_{\text{abs}}$  ranges, so that all systems averaged include coverage of all the lines to be compared.

For studying the dust content of the absorbers by its effect on the QSO continua, geometric mean QSO spectra in the absorber rest frame were generated. The procedure for generating the geometric mean spectra is similar to that for the arithmetic mean spectra, except that the individual spectra were not normalized, and the arithmetic means of the logarithmic flux densities of the nonmasked pixels were calculated (producing geometric means in linear flux density). For each absorber subsample composite spectrum, a geometric mean spectrum was generated for a QSO sample matched in SDSS  $i$  magnitude and QSO redshift, but without absorption-line systems of grades A, B, or C in their spectra. The matching of  $z_{\text{em}}$  and  $i$  magnitude means that the absolute  $i$  magnitudes of the absorber and nonabsorber pair also match. The matched nonabsorber spectra were shifted in the

TABLE 1  
SAMPLE DEFINITIONS AND PROPERTIES

Sample No.	Selection Criterion	$E(B-V)$	No. Systems	$\langle W_{\text{Mg II}} \rangle$ (Å)	$\langle z_{\text{abs}} \rangle$	$\langle \beta \rangle$	$\langle i \rangle^a$	$\langle M_i \rangle^b$	$\Delta(g-i)^c$
1.....	Full sample	$0.026 \pm 0.004$	415	1.54	1.48	0.0018	18.61	-26.52	0.124
2.....	$M_{i < -26.49}$	$0.024 \pm 0.008$	208	1.37	1.62	0.0019	18.31	-27.08	0.082
3.....	$M_{i \geq -26.49}$	$0.034 \pm 0.006$	207	1.70	1.35	0.0019	18.92	-25.95	0.166
4.....	$W_{\text{Mg II}} < 1.35 \text{ \AA}$	$0.018 \pm 0.005$	208	0.86	1.51	0.0017	18.49	-26.70	0.087
5.....	$W_{\text{Mg II}} \geq 1.35 \text{ \AA}$	$0.034 \pm 0.003$	207	2.23	1.46	0.0020	18.74	-26.34	0.161
6.....	$\beta < 0.0$	$0.035 \pm 0.004$	152	1.54	1.49	-0.0027	18.58	-26.54	0.140
7.....	$0.0 \leq \beta < 0.01$	$0.020 \pm 0.005$	263	1.54	1.48	0.0045	18.63	-26.51	0.115
8.....	$\beta < -0.0022$	$0.033 \pm 0.006$	74	1.65	1.57	-0.0045	18.45	-26.82	0.132
9.....	$-0.0022 \leq \beta < 0.0$	$0.038 \pm 0.006$	78	1.43	1.41	-0.0011	18.70	-26.27	0.148
10.....	Radio-detected (RD)	$0.086 \pm 0.003^d$	48	1.90	1.39	0.0012	18.60	-26.35	0.359
11.....	Radio-undetected (RUD)	$0.016 \pm 0.004^c$	318	1.52	1.50	0.0019	18.63	-26.52	0.094
12.....	$z_{\text{abs}} > 1.4675, \beta < 0.01$	$0.025 \pm 0.003$	250	1.47	1.65	0.0019	18.64	-26.80	0.114
13.....	$z_{\text{abs}} > 1.4675, \text{ positive } \beta$	$0.021 \pm 0.005$	156	1.48	1.65	0.0049	18.69	-26.76	0.114
14.....	$z_{\text{abs}} > 1.4675, \text{ negative } \beta$	$0.031 \pm 0.005$	94	1.46	1.65	-0.0032	18.57	-26.86	0.115
SY06.....	Sample 1, from Y06 <sup>f</sup>	0.013	809	1.73	1.33	0.120	18.96	-26.43	0.042
SY06CIV.....	SY06 with $z_{\text{abs}} > 1.4675$	0.015	250	1.69	1.61	0.064	18.99	-26.66	0.051
SY06RD.....	Radio-detected, from SY06	0.037	41	1.98	1.31	0.11	19.09	-26.29	0.16
SY06RUD.....	Radio-undetected, from SY06	0.015	614	1.73	1.34	0.12	19.05	-26.42	0.035

<sup>a</sup> SDSS  $i$  magnitude, corrected for Galactic extinction.

<sup>b</sup> Absolute  $i$  magnitude, using the concordance cosmology.

<sup>c</sup>  $\Delta(g-i)$  for absorber sample [ $\sim 4E(B-V)$ ; see text].

<sup>d</sup> Restricting the matched nonabsorber comparison sample to radio-detected QSOs reduces the value of  $E(B-V)$  to  $0.062 \pm 0.007$ .

<sup>e</sup> Restricting the matched nonabsorber comparison sample to radio-undetected QSOs increases the value of  $E(B-V)$  to  $0.018 \pm 0.007$ .

<sup>f</sup> This sample uses the same selection criterion as the sample 1 of associated systems, but has  $\beta > 0.01$ .

procedure to the same rest frames as their absorption sample counterparts, to produce composite nonabsorber spectra that can be compared directly to the composite absorber spectra. There are 9737 QSOs in the SDSS DR3 data set available for use in the matched nonabsorber samples in the redshift range of interest here; they are free of detected absorption systems, but otherwise satisfy the same selection criteria as QSOs in the absorber sample. The details of the selection of the matching nonabsorber sample are described in Y06. The list of QSOs in the set of best-matched nonabsorbers spectra (for the full absorber sample 1) is given in Table 5 of the Appendix.

The ratio of the geometric mean composite spectra of the absorber sample to that of the nonabsorber sample is the relative shape of the back-lighting QSO continua, with and without absorption systems. We interpret the ratio as the extinction curve due to dust associated with the absorption systems. It was shown by Y06 that these ratios, produced using various subsamples of intervening absorption-line systems, can be well fit by an SMC extinction law, with different values of the color excess  $E(B-V)$ . In the same way, we fit SMC extinction curves to the geometric mean spectra ratios for our current samples, to derive values of  $E(B-V)$  for associated systems. In none of the absorber samples did a Milky Way type extinction curve provide a better fit, and we report only the results for the SMC type fits.

To assess the uncertainty of the relative extinction curves and the derived values of  $E(B-V)$ , five independent (without any QSOs in common) matching nonabsorber samples were selected for each absorber sample.<sup>7</sup> The first nonabsorber sample (given in Table 5 of the Appendix) selects the closest matching (in  $z_{\text{em}}$  and  $i$  magnitude) nonabsorber QSOs. The subsequent non-

absorber samples use the QSOs with the next best matches not already used in the previous nonabsorber samples. The largest average differences between the  $z_{\text{em}}$  and  $i$  magnitude of the absorber and nonabsorber QSOs in the fifth nonabsorber sample are  $\langle \Delta z \rangle = 0.03$  and  $\langle |\Delta i| \rangle = 0.07$ . Composite spectra were constructed and  $E(B-V)$  values were obtained for each of the five nonabsorber samples for the absorber sample. The five values of  $E(B-V)$  were averaged to define the  $E(B-V)$  of the absorber sample. The rms dispersion of the five samples (of order  $\pm 0.004$  mag, attributable to sample selection randomness) was used as a measure of the uncertainty in the values of  $E(B-V)$ . The derived values of  $E(B-V)$  and the associated uncertainties are given in Table 1 for each absorber subsample. We conclude that for comparison of extinctions between our subsamples, differences of 0.01 in  $E(B-V)$  are significant and are not caused by systematic errors in defining the continuum. It is possible that a few of the nonabsorber QSOs have high intrinsic extinction, and the presence of such QSOs in a nonabsorber sample will reduce the value of  $E(B-V)$ . The use of five independent nonabsorber samples for determining the  $E(B-V)$  values minimizes the effect of such rare nonabsorber QSOs. The subsamples are described next in § 2.3.

### 2.3. Subsample Definitions

The full sample (sample 1) was divided into several subsamples based on the absorber and QSO properties to study the dependence of the dust content, ionization properties, and relative abundances on these properties. The subsamples were initially defined based on dividing the full sample by absolute  $i$  magnitude,<sup>8</sup> Mg II equivalent width,  $\beta$  (positive or negative), negative  $\beta$  (further divided into two), and radio detection/nondetection by the VLA FIRST survey. Specifically, we divided

<sup>7</sup> The sample of Y06 was based on the SDSS DR1, for which there were fewer QSOs than we find in DR3 and for which we could not find enough QSOs without absorption lines to test the dispersion in color excess for the effects of random differences in the QSO continua.

<sup>8</sup> Determined by using the so-called ‘‘concordance cosmology’’ ( $\Omega_m = 0.3$ ,  $\Omega_l = 0.7$ ,  $H_0 = 70 \text{ km s}^{-1} \text{ Mpc}^{-1}$ ).

sample 1 into pairs of subsamples in three different ways: by absolute  $i$  magnitude, at the median value of  $-26.49$  (Nos. 2 and 3); by  $W_{\text{Mg II}}$ , at the median value of  $1.35 \text{ \AA}$  (Nos. 4 and 5); and by  $\beta < 0$  or  $> 0$  (Nos. 6 and 7). Sample 6 was further subdivided into two subsamples at the median  $\beta$  value of  $-0.0022$  (Nos. 8 and 9).

In order to study the dependence of the properties of the associated absorbers on the radio properties of the QSOs, the full sample was divided into subsamples based on the detection or nondetection of the QSOs by the FIRST survey (for those QSOs covered by the FIRST survey); these subsamples are designated No. 10 (hereafter RD [radio-detected] QSOs) and No. 11 (hereafter RUD [radio-undetected] QSOs). The completeness limit of the FIRST survey catalog across the survey area is  $1 \text{ mJy}$  (Becker et al. 1995); undetected QSOs have  $20 \text{ cm}$  fluxes less than this value. Miller et al. (1990) define radio-loud QSOs to be those having  $1.4 \text{ GHz}$  luminosities greater than  $10^{25} \text{ W Hz}^{-1}$ . Thus, the RD QSOs with  $z_{\text{em}} < 2.0$  in the FIRST survey are radio-loud. As all the QSOs in our sample have  $z_{\text{em}} < 1.96$ , our radio-detected and radio-undetected subsamples can be considered to be subsamples of radio-loud and radio-quiet QSOs according to the definition of Miller et al. (1990).

In order to study the difference in ionization state (measured by the strength of the C IV absorption lines compared to the Mg II absorption lines) of the associated ( $\beta < 0.01$ ) and intervening ( $\beta > 0.01$ ) systems, we constructed a subsample (No. 12) of associated systems with  $z_{\text{abs}} > 1.4675$ , so that the wavelength of the C IV lines would be covered by the SDSS spectrum.<sup>9</sup> Subsample 12 was subdivided into two parts (Nos. 13 and 14) depending on  $\beta$  being  $>$  or  $<$  0.

The required subsamples of intervening systems, for comparison, are as follows. Y06 compiled a sample of 809 intervening systems (hereafter SY06) satisfying the same criteria for selection as used here, except having  $\beta > 0.01$ . This forms our main sample of intervening absorbers. For ionization studies, we selected a subsample of SY06 having  $z_{\text{abs}} > 1.4675$  (subsample SY06CIV). We also defined subsamples based on radio detection or non-radio-detection, from the Y06 intervening sample, for comparison with the associated sample. These two samples are referred to as SY06RD and SY06RUD, respectively.

Properties of various subsamples (including those of intervening samples) are listed in Table 1, which includes the defining criteria, the average and rms dispersion of  $E(B-V)$  values obtained using the five independent, nonabsorber samples, along with the average values of  $W_{\text{Mg II}}$ ,  $\beta$ ,  $z_{\text{abs}}$ ,  $i$  magnitude, absolute  $i$  magnitude calculated using the concordance cosmology, and  $\Delta(g-i)$ .

### 3. RESULTS

#### 3.1. Comparison of Properties of Intervening and Associated Systems

To compare the properties of the associated (sample 1) and the intervening (SY06) systems, we have plotted in Figure 2 the distribution of  $W_{\text{Mg II}}$ ,  $W_{\text{Mg I}}/W_{\text{Mg II}}$ , the doublet ratio of Mg II,  $W_{\text{Al II}}/W_{\text{Al III}}$ , and absolute  $i$  magnitudes for the two samples (left side of the Figs. 2a–2e). The ionization measure,  $W_{\text{C IV}}/W_{\text{Mg II}}$ , for the associated (No. 12) and intervening (SY06CIV) subsamples is shown in the left side of Figure 2f (recall that both these subsamples have spectra which cover both C IV and Mg II doublets). Here,  $W_{\text{Mg I}}$ ,  $W_{\text{Al II}}$ ,  $W_{\text{Al III}}$ , and  $W_{\text{C IV}}$  are the rest-frame equivalent widths of Mg I  $\lambda 2852$ , Al II  $\lambda 1670$ , Al III  $\lambda 1854$ , and

C IV  $\lambda 1548$ , respectively, in  $\text{\AA}$ . We use vacuum wavelengths throughout, and truncate the values in our ion notation. In making these plots we have used only systems for which the equivalent widths of the lines are significant at more than the  $4\sigma$  level. For subsample 12, C IV lines were below  $4\sigma$  for 26 systems, of the 250 total systems in the subsample. The upper limits on  $W_{\text{C IV}}/W_{\text{Mg II}}$  for these systems are  $< 0.8$ . Thus, they will mostly fall within the first two bins. Similarly, for the SY06CIV subsample, the C IV lines were not detected at  $4\sigma$  significance for 52 systems. The upper limits on  $W_{\text{C IV}}/W_{\text{Mg II}}$  for these systems are  $< 0.5$ , and these systems will lie in the first two bins. We have also plotted in Figure 2 the distributions for associated systems with positive and negative  $\beta$  (subsamples 7 and 6, on the right of Figs. 2a–2e; subsamples 13 and 14, on the right of Fig. 2f).

Qualitatively, it is clear from Figure 2 that, while the distribution for two parameters, the Mg II doublet ratio and the absolute  $i$  magnitude, are similar between the associated and intervening samples, those for the three ion ratios compared, and for the Mg II equivalent widths, are not. These conclusions also seem to apply to the samples with positive and negative  $\beta$  values.

We have performed a number of statistical tests to determine the probabilities that the quantities plotted in Figure 2, the equivalent width of C IV  $\lambda 1548$  and the doublet ratio for C IV, for the intervening and associated systems, and also for subsamples 7 and 6, are drawn from the same distributions. We have performed the KS test for three cases: (1) taking only the measured values of various quantities and ignoring the nondetections, (2) assuming the values for the nondetections to be zero, and (3) assuming the values for the nondetections to be equal to  $3\sigma$  values. The actual result should be bracketed by these cases, in particular cases 2 and 3. In addition, to directly account for the upper limits, we have used two commonly employed tests from survival analysis statistics, namely the Gehan and log-rank tests, which are described in astronomical nomenclature by Feigelson & Nelson (1985). Like the KS test, both survival analysis tests are designed to compare the distributions of a parameter measured in two samples; unlike the KS test, they take the upper limits within the distributions into account. Both survival analysis tests give similar results when applied to the current data sets. The results of these tests are given in Table 2. These show that the doublet ratios of Mg II and C IV and the absolute magnitudes of associated and intervening systems are drawn from the same distributions, indicating a similar degree of saturation of the Mg II and C IV lines for these two types of systems. These conclusions are also valid for the two samples with positive and negative  $\beta$  values. The equivalent width distribution for Mg II differs for the comparison of associated to intervening samples, but not for the two associated samples. The  $W_{\text{C IV}}/W_{\text{Mg II}}$  ratios, and possibly the  $W_{\text{Mg I}}/W_{\text{Mg II}}$  ratios, for the associated and intervening systems are different, indicating a difference in ionization levels of the two types of systems, the associated systems being more highly ionized than the intervening systems (see Fig. 2). The situation is not so clear for the  $W_{\text{Al II}}/W_{\text{Al III}}$  ratio, for which the KS test and the survival analysis tests give very different results.

The dependence of ionization on  $\beta$  is less clear. The results of KS tests for  $W_{\text{C IV}}/W_{\text{Mg II}}$  and  $W_{\text{Mg I}}/W_{\text{Mg II}}$  do indicate a difference in ionization levels, the negative  $\beta$  systems being more highly ionized than the positive  $\beta$  systems (see Fig. 2). However, the survival analysis results do not corroborate this. The distribution of  $W_{\text{C IV}}$  is, however, very different for the two samples.

The ratio  $W_{\text{Mg I}}/W_{\text{Mg II}}$  is enhanced among the associated systems compared to the intervening systems for ratios near 0.6 (SY06),

<sup>9</sup> This sample is also definitely free of classic C IV, BAL systems, which as previously noted, cannot be assured for the lower  $z$  systems.

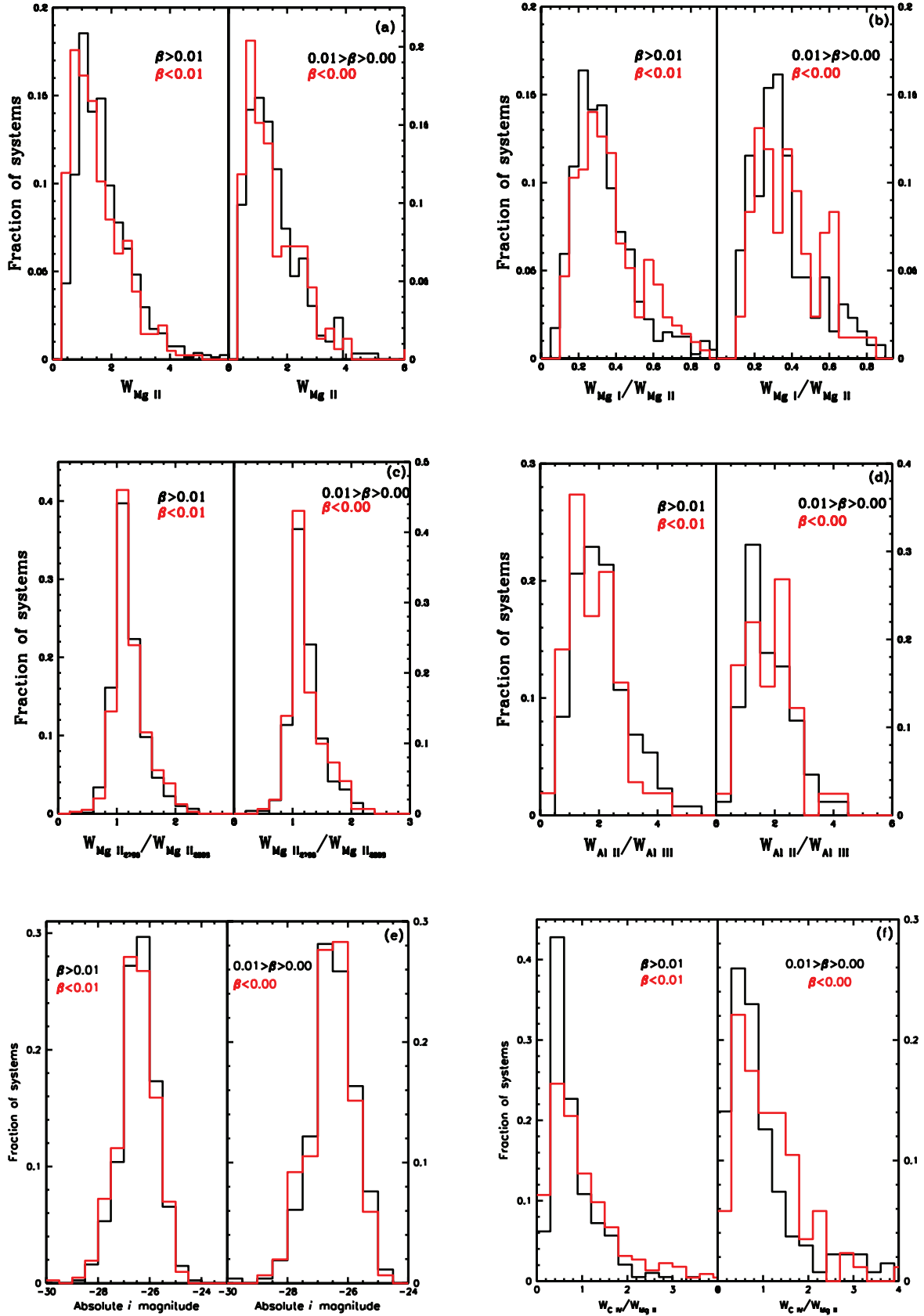


FIG. 2.—Histograms comparing properties of associated (sample 1, this paper;  $\beta < 0.01$ , red) and intervening (SY06;  $\beta > 0.01$ , black) systems appear on the left of five subpanels which show (a)  $W_{\text{Mg II}}$ ; (b)  $W_{\text{Mg I}}/W_{\text{Mg II}}$ ; (c) the Mg II doublet ratio; (d)  $W_{\text{Al II}}/W_{\text{Al III}}$ ; and (e) absolute  $i$  magnitude. Panel f shows the ratio  $W_{\text{C IV}}/W_{\text{Mg II}}$ , taken as an indicator of ionization. The left side of that panel compares the sample of associated systems (subsample 12;  $\beta < 0.01$ , red) with the intervening systems from Y06 (subsample SY06CIV;  $\beta > 0.01$ , black), that is the subsamples with complete coverage of C IV doublets. The right side of panels a–e show the positive (black) and negative (red)  $\beta$ -associated systems from sample 1 (subsamples 6 and 7) of this paper. The right side of panel f shows positive (subsample 13; black) and negative (subsample 14; red)  $\beta$  subsamples for the Mg II systems from the associated systems in subsample 12 of this paper (complete in C IV).

TABLE 2  
RESULTS OF STATISTICAL TESTS

VARIABLE	ASSOCIATED/INTERVENING			POSITIVE/NEGATIVE $\beta$		
	Samples	KS Test <sup>a</sup>	Survival Analysis <sup>b</sup>	Samples	KS Test <sup>c</sup>	Survival Analysis <sup>d</sup>
$W_{\text{Mg II}}$ .....	1, SY06	0.00	0.00, 0.00	6, 7	0.43	0.46, 0.51
Mg II doublet ratio .....	1, SY06	0.12	0.26, 0.39	6, 7	0.53	0.78, 0.68
$W_{\text{Mg I}}/W_{\text{Mg II}}$ .....	1, SY06	0.01, 0.00, 0.36	0.01, 0.05	6, 7	0.03, 0.00, 0.12	0.26, 0.11
$W_{\text{Al II}}/W_{\text{Al III}}$ .....	1, SY06	0.10, 0.00, 0.00	0.70, 0.62	6, 7	0.45, 0.34, 0.55	0.76, 0.93
$W_{\text{C IV}}/W_{\text{Mg II}}$ .....	12, SY06CIV	0.00, 0.00, 0.00	0.00, 0.00	13, 14	0.04, 0.05, 0.05	0.13, 0.39
$W_{\text{C IV}}$ .....	12, SY06CIV	0.05, 0.00, 0.00	0.12, 0.08	6, 7	0.08, 0.09, 0.15	0.06, 0.07
C IV doublet ratio .....	12, SY06CIV	0.77, 0.68, 0.58	0.15, 0.14	6, 7	0.62, 0.92, 0.82	0.25, 0.42
Absolute $i$ magnitude .....	1, SY06	0.13	0.21, 0.25	6, 7	0.96	0.07, 0.10

NOTE.—Probability values smaller than  $5 \times 10^{-3}$  have been given as 0.

<sup>a</sup> Probability that the associated and intervening samples (left panels of Figs. 2a–2f and the equivalent width of C IV  $\lambda$ 1548) are drawn from the same distribution. Three numbers in this column (which should bracket the actual result) indicate KS test probabilities for the cases in which (1) nondetections have been excluded, (2) nondetections are treated as having zero equivalent width, and (3) nondetections are replaced by  $3\sigma$  values, respectively; a single entry is given for the quantities whose values are available for all the systems.

<sup>b</sup> Probability that the associated and intervening samples (left panels of Figs. 2a–2f and the equivalent width of C IV  $\lambda$ 1548) are drawn from the same distribution. The two numbers are for Gehan test and the log-rank test, respectively. These tests include the  $3\sigma$  upper limits.

<sup>c</sup> Probability for samples with positive and negative  $\beta$  (right panels of Figs. 2a–2f and the equivalent width of C IV  $\lambda$ 1548) to be drawn from the same distribution. The three numbers are for cases described in footnote a.

<sup>d</sup> Probability for samples with positive and negative  $\beta$  (right panels of Figs. 2a–2f and the equivalent width of C IV  $\lambda$ 1548) to be drawn from the same distribution. The two numbers are for Gehan test and the log-rank test, respectively. These tests include the  $3\sigma$  upper limits.

evidently mainly because of the contribution of systems with  $\beta < 0$ , so the statistical tests give a low probability of the compared distributions being the same. This feature could represent an enhancement of Mg I owing to higher density in the negative  $\beta$  systems, a different temperature (affecting the recombination rate of Mg I; York & Kinahan 1979), or a specific effect of the ionization field near 1100 Å (the ionization limit of Mg I). (It was found by Y06 that the blend of components that constitutes the Mg I feature typically technically saturated at  $W \sim 0.6$  Å, which could be related to the excess seen here.)

### 3.2. Line Strengths in the Composite Spectra

Equivalent widths of the measured lines in the arithmetic mean composite spectrum for the full sample (No. 1) are given in column (4) of Table 3. Also given, in column (5), are the equivalent widths of the lines for the sample of intervening systems (SY06) as obtained by Y06. To the left are the vacuum wavelengths, the species, and the intrinsic strength indicator,  $f\lambda^2/10^4$ . While the equivalent widths of the Mg II  $\lambda\lambda$ 2796, 2890 and Al II  $\lambda$ 1670 lines are similar, the C IV  $\lambda\lambda$ 1548, 1550, Si IV  $\lambda\lambda$ 1396, 1402, and Al III  $\lambda\lambda$ 1854, 1862 (marginally) lines are stronger in the associated sample than in the intervening sample. However, as noted above, because of the selected range of  $z_{\text{em}}$ , the composite spectrum gets a contribution from all absorbers only for lines with rest-frame wavelength in the range 1900–3150 Å. All the systems in subsamples 12 and SY06CIV, by construction, contribute to the composite spectrum between wavelengths 1540 and 3150 Å. The equivalent widths of various lines for these two subsamples are given in columns (6) and (7) of Table 3. The arithmetic mean composite spectra of the two subsamples is shown in Figure 3. It can be seen that the higher ionization C IV lines are indeed stronger and the lower ionization lines (Mg II, Fe II, Al II, Si II) are weaker in the associated systems as compared to those in the intervening systems, consistent with the earlier conclusion that the ionization is higher in associated systems.

In order to determine if the ionization level in associated systems depends on  $\beta$ , we measured the equivalent widths of lines in the composite spectra of subsamples 13 and 14. These are also given in Table 3, columns (8) and (9), respectively. There is

definite evidence of higher ionization for lower  $\beta$  values. The average absolute  $i$  magnitudes of these two subsamples ( $-26.76$  and  $-26.86$  for Nos. 13 and 14, respectively) differ only by 0.1, and the distribution of absolute  $i$  magnitudes is similar (KS test probability that they are drawn from the same distribution being 0.13), so that the difference in ionization is not caused by different intrinsic ionizing fluxes of the QSOs.

It has been found that, in a few QSOs, the absorbing material giving rise to the associated systems covers the continuum source in the QSO only partially (e.g., Barlow & Sargent 1997; Hamann et al. 1997a). This can complicate the interpretation of the observed equivalent widths. The partial coverage of the source will change the doublet ratios of the absorption lines. The two lines of the C IV doublet are not completely resolved (detached) in our composite spectra. However, the distributions of the doublet ratios of Mg II lines for the intervening and associated samples, as well as the subsamples with different  $\beta$  ranges, are very similar (see Fig. 2 and Table 2). The equivalent widths and line profiles of Mg II lines in sample 1 and SY06 are also very similar. So the issue of covering factor may not be very important. Also, the equivalent widths of lines of C IV and Mg II differ in opposite senses in subsamples with different  $\beta$  values. Thus, we believe that our interpretation of higher ionization in associated absorbers as compared to the intervening systems and its dependence on  $\beta$  in associated absorbers is justified.

The strongest lines in Figure 3 undoubtedly consist of many components, some saturated and some not. To understand the detailed behavior of the composite spectra will require high-resolution observations of a number of individual systems, to fully sort out the effects of saturation, any dilution by low covering factors that may exist in some cases, and blending of many components. Such a program has already been undertaken for the intervening sample (Meiring et al. 2006; Peroux et al. 2006); differences between that sample and an associated sample observed in the same way will be very useful for understanding the associated systems. However, the global ionization effects noted here, from equivalent width ratios of the strong lines (of C IV and Mg II), which show consistent behavior among various subsamples, should not change.

TABLE 3  
EQUIVALENT WIDTHS FOR SELECTED SAMPLES

$\lambda$	SPECIES	$f\lambda^2/10^{4a}$	EQUIVALENT WIDTH WITH 1 $\sigma$ ERRORS (mÅ; upper limits are 3 $\sigma$ values)					
	Subsample number:		1	SY06	12	SY06CIV	13	14
	$\beta$ :		<0.01	>0.01	<0.01	>0.01	0.0–0.01	<0
	Number of systems:		415	809	250	250	156	94
1548.20.....	C IV	45.5	1146 $\pm$ 8	839 $\pm$ 10	1148 $\pm$ 8	855 $\pm$ 8	1131 $\pm$ 13	1216 $\pm$ 22
1550.78.....	C IV	22.8	880 $\pm$ 8	580 $\pm$ 9	881 $\pm$ 8	625 $\pm$ 7	738 $\pm$ 13	1082 $\pm$ 23
2852.96.....	Mg I	1489	252 $\pm$ 4	282 $\pm$ 4	213 $\pm$ 6	261 $\pm$ 7	201 $\pm$ 7	224 $\pm$ 11
2796.35.....	Mg II	482	1388 $\pm$ 6	1432 $\pm$ 4	1167 $\pm$ 8	1465 $\pm$ 9	1228 $\pm$ 10	1112 $\pm$ 12
2803.53.....	Mg II	241	1248 $\pm$ 6	1261 $\pm$ 4	1102 $\pm$ 8	1255 $\pm$ 9	1134 $\pm$ 10	1075 $\pm$ 12
1670.79.....	Al II	486	464 $\pm$ 6	471 $\pm$ 6	431 $\pm$ 8	455 $\pm$ 6	430 $\pm$ 8	442 $\pm$ 10
1854.72.....	Al III	192	229 $\pm$ 4	183 $\pm$ 4	240 $\pm$ 6	201 $\pm$ 7	208 $\pm$ 8	269 $\pm$ 9
1862.79.....	Al III	97	128 $\pm$ 7	112 $\pm$ 4	131 $\pm$ 6	111 $\pm$ 6	112 $\pm$ 9	132 $\pm$ 10
1808.00.....	Si II	0.69	53 $\pm$ 5	68 $\pm$ 5	52 $\pm$ 5	57 $\pm$ 4	46 $\pm$ 7	61 $\pm$ 8
1393.32.....	Si IV	99.7	890 $\pm$ 28	<sup>b</sup>	900 $\pm$ 26	380 $\pm$ 19	581 $\pm$ 23	1423 $\pm$ 45
1402.77.....	Si IV	50	605 $\pm$ 20	<sup>b</sup>	608 $\pm$ 19	324 $\pm$ 15	300 $\pm$ 23	1100 $\pm$ 46
1526.71.....	Si II	31	473 $\pm$ 7	383 $\pm$ 10	471 $\pm$ 7	397 $\pm$ 9	404 $\pm$ 10	556 $\pm$ 11
2056.26.....	Cr II	43.6	22 $\pm$ 4	39 $\pm$ 4	23 $\pm$ 4	23 $\pm$ 4	26 $\pm$ 8	23 $\pm$ 8
2062.24.....	Cr II	32.4	19 $\pm$ 3 <sup>c</sup>	27	19 $\pm$ 4 <sup>c</sup>	40 $\pm$ 3 <sup>c</sup>	33 $\pm$ 8 <sup>c</sup>	21 $\pm$ 7 <sup>c</sup>
2066.16.....	Cr II	21.7	<11	14 $\pm$ 4	14 $\pm$ 4	17 $\pm$ 3	<18	<24
2576.88.....	Mn II	240	52 $\pm$ 4	54 $\pm$ 4	51 $\pm$ 4	64 $\pm$ 6	42 $\pm$ 6	74 $\pm$ 8
2594.50.....	Mn II	188	33 $\pm$ 3	50 $\pm$ 4	17 $\pm$ 4	44 $\pm$ 8	25 $\pm$ 6	<15
2606.46.....	Mn II	135	23 $\pm$ 2	26 $\pm$ 4	9 $\pm$ 3	24 $\pm$ 7	27 $\pm$ 6	10 $\pm$ 3
2382.77.....	Fe II	182	760 $\pm$ 8	761 $\pm$ 4	674 $\pm$ 8	672 $\pm$ 5	607 $\pm$ 11	761 $\pm$ 8
2600.17.....	Fe II	162	709 $\pm$ 3	783 $\pm$ 4	597 $\pm$ 4	736 $\pm$ 8	667 $\pm$ 6	517 $\pm$ 7
2344.21.....	Fe II	62.6	486 $\pm$ 4	550 $\pm$ 4	413 $\pm$ 7	457 $\pm$ 4	415 $\pm$ 7	424 $\pm$ 11
2586.65.....	Fe II	46	428 $\pm$ 3	509 $\pm$ 4	343 $\pm$ 4	475 $\pm$ 8	382 $\pm$ 6	297 $\pm$ 6
2374.46.....	Fe II	17.6	259 $\pm$ 5	298 $\pm$ 4	214 $\pm$ 6	257 $\pm$ 6	220 $\pm$ 9	213 $\pm$ 10
1608.45.....	Fe II	14.9	128 $\pm$ 5	$\pm$	121 $\pm$ 5	210 $\pm$ 7	131 $\pm$ 6	111 $\pm$ 8
2260.78.....	Fe II	1.2	43 $\pm$ 4	46 $\pm$ 4	34 $\pm$ 5	34 $\pm$ 7	25 $\pm$ 7	51 $\pm$ 11
2249.88.....	Fe II	0.9	35 $\pm$ 5	35 $\pm$ 4	19 $\pm$ 4	13 $\pm$ 4	<18	34 $\pm$ 9
2367.59.....	Fe II	0.012	<7	<8	<9	<13	<16	<21
2012.17.....	Co II	15	12 $\pm$ 4	15 $\pm$ 4	<16	12 $\pm$ 3	<25	<18
1941.29.....	Co II	12.8	<8	<8	<12	<10	<12	<20
1741.55.....	Ni II	13	33 $\pm$ 4	28 $\pm$ 4	32 $\pm$ 5	<24	34 $\pm$ 8	28 $\pm$ 6
1709.60.....	Ni II	9.4	22 $\pm$ 4	16 $\pm$ 4	19 $\pm$ 3	12 $\pm$ 3	13 $\pm$ 3	<13
1751.92.....	Ni II	8.6	26 $\pm$ 4	<6	21 $\pm$ 4	10 $\pm$ 3	33 $\pm$ 8	<9
2026.14.....	Zn II <sup>c</sup>	205	46 $\pm$ 5	48 $\pm$ 4	44 $\pm$ 6	36 $\pm$ 3	30 $\pm$ 5	59 $\pm$ 11
2062.66.....	Zn II	105	19 $\pm$ 3 <sup>c</sup>	22	19 $\pm$ 4 <sup>c</sup>	40 $\pm$ 3 <sup>c</sup>	33 $\pm$ 8 <sup>c</sup>	21 $\pm$ 6 <sup>c</sup>

<sup>a</sup> This is the relative strength for lines of the same species and can be used to indicate the degree of saturation present. For instance, for sample 1,  $W_{\text{Al II}}/W_{\text{Al III}} = 1.8$ , whereas the ratio in col. (3) is 2: on average, the doublet lines of Al III are only slightly saturated.

<sup>b</sup> These equivalent widths were not listed in Y06.

<sup>c</sup> These lines are blended with lines of other species.

In Figure 4 we show profiles of a few selected lines in various subsamples of associated systems. It can be seen that most lines are stronger in the subsample comprising intrinsically faint QSOs (No. 3) as compared to those in the subsample comprising intrinsically bright QSOs (No. 2) (the average observed  $i$  magnitudes for the two subsamples also differ considerably). This was also observed by Y06 for the intervening systems, and was understood as being the effect of lower S/N in the spectra of faint QSOs, which makes only relatively stronger absorption systems in these QSOs detectable at the 4  $\sigma$  level. As expected, all the lines are stronger in the subsample of stronger Mg II systems (No. 5) as compared to those in the subsample of weaker Mg II systems (No. 4). As noted above, lines of higher ionization are stronger in the subsample (No. 6) of smaller  $\beta$  compared to those in the subsample (No. 7) of larger  $\beta$  values. Finally, all of the lines are stronger in the subsample (No. 10) of RD QSOs as compared to those in the subsample (No. 11) of RUD QSOs. This appears to be due to the fact that subsample 10 comprises stronger Mg II systems, having average  $W_{\text{Mg II}} = 1.9$  Å, compared to 1.52 Å for subsample 11. One of the systems in sub-

sample 10 has very high  $W_{\text{Mg II}}$  ( $\sim 9$  Å). This contributes significantly to the equivalent widths of most lines in the composite spectrum of the subsample.

The strong ionization effect noted in C IV is even more noticeable in Si IV (Table 3, Figs. 3 and 4, row 4). This could be an effect of just a few peculiar systems with high enough redshift to contribute to both samples 1 and 12. To check this, we formed a sample of systems with  $z_{\text{abs}} > 1.7378$ , so that Si IV was completely covered in all cases, along with C IV and Mg II. The same trends evident in Table 3 persist. For respective subsamples of (1) intervening systems (from Y06); (2) associated, positive  $\beta$  systems; and (3) associated, negative  $\beta$  systems, all with  $z_{\text{abs}} > 1.7378$ , the values of the equivalent widths of Si IV  $\lambda 1393$  are 380, 590, and 1330 mÅ, while for  $W_{\text{C IV}}$  we find 880, 1060, and 1320 mÅ, respectively. These values are within 10% of the corresponding number from subsamples 12, 13, and 14 in Table 3, so the effect does seem to be real. That is, the Si IV lines are relatively stronger as the systems have lower and lower  $\beta$ . The number of systems in these subsamples are only 35, 27, and 45, so this result needs to be confirmed in much larger samples (e.g., SDSS DR5).

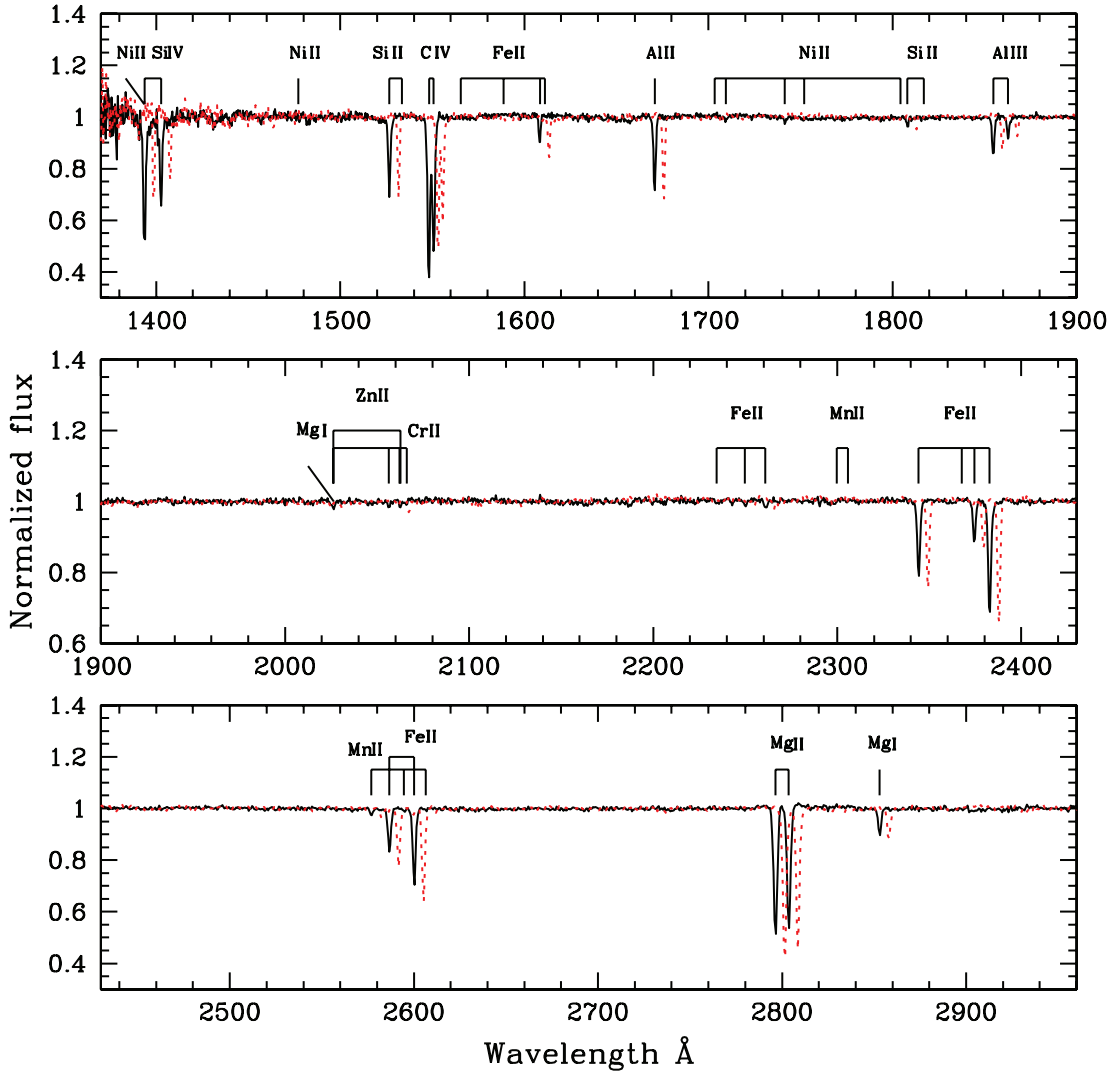


FIG. 3.—Arithmetic mean composite spectrum of the systems in the subsample (No. 12) of associated systems having  $z_{\text{abs}} > 1.4675$  (so that the SDSS spectrum includes the C IV doublet) in the absorber rest frame (black solid line). Individual spectra have been normalized using the first 30 eigenspectra of the principle components of the QSO spectra and weighted by inverse variance. All spectra contribute to the region between 1540 and 3150 Å, which therefore has a high S/N. A similar spectrum for intervening absorbers (subsample SY06CIV; red dotted line) culled from SY06 is shown for comparison. This spectrum is shifted by 5 Å to the right for ease in visual comparison. Please note the different y-axis scale in the middle panel. The wavelength scale is uniform, so lines of a given velocity width appear broader at longer wavelengths.

### 3.3. Extinction

The geometric mean composite spectrum for the full sample (No. 1) is given in Figure 5. Also plotted is the composite spectrum for the matching nonabsorber sample. In the bottom panel of the figure we have plotted the ratio of the two composites, the best-fit SMC extinction curve, and the Milky Way extinction curve for the same value of  $E(B - V)$ . Similar to the case of intervening systems (Y06), no 2175 Å bump is seen in the observed spectrum. The bump is not present in the composite spectrum of any of the subsamples either, and the SMC extinction curve appears to describe the observed extinction curve reasonably well. This is also supported by the fact that the  $E(B - V)$  values are close to 0.25 times the average values of  $\Delta(g - i)$  for the subsamples (see Table 1). Such a relationship was discovered by Y06 for the subsamples of intervening systems, which also seemed to be well described by an SMC type of extinction curve. The lack of evidence for a significant 2175 Å bump is consistent with the fact that the feature has been detected in the spectra of only a small number of individual QSOs (e.g.,

Motta et al. 2002; Wang et al. 2004; Junkkarinen et al. 2004; Mediavilla et al. 2005; see additional comments in Y06).

By contrast to the case of intervening systems (Fig. 2 of Y06 for instance), the composite spectra for the associated systems (top panel of our Fig. 5) show typical QSO emission lines. This is due to the fact that for associated systems, the absorption redshifts are very close to the emission redshifts, and the emission lines in individual spectra are very nearly aligned even in the absorber rest frames. In the extinction curves (bottom panel of Fig. 5), there appears to be some emission present at the wavelengths of [C III] and Mg II lines, and possibly those of other QSO emission lines. This could be due to either the emission by the absorbers, or an artificial effect produced by the small differences in the emission redshifts of the absorber and non-absorber QSOs. From Figure 5 one also gets the impression that the shape of the emission lines in the absorber and nonabsorber spectra are different. In order to understand these effects, we produced geometric mean composite spectra of the absorber and nonabsorber samples in the rest frame of the QSOs. The ratio of these two composites did not show any emission. This

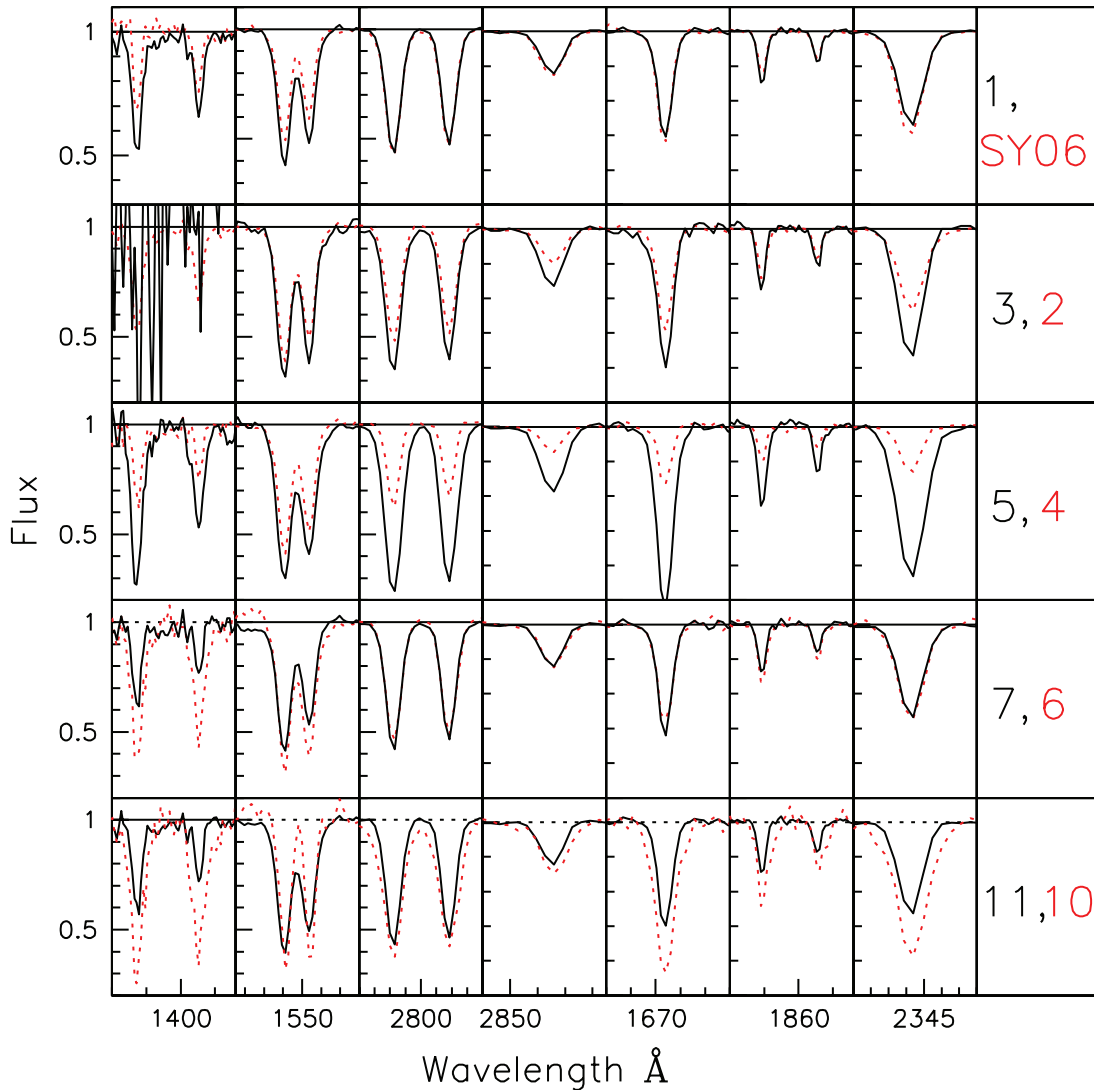


FIG. 4.— Comparison of profiles of absorption lines Si IV  $\lambda\lambda$ 1393, 1402, C IV  $\lambda\lambda$ 1548, 1550, Mg II  $\lambda\lambda$ 2796, 2803, Mg I  $\lambda$ 2852, Al II  $\lambda$ 1670, Al III  $\lambda\lambda$ 1854, 1864, and Fe II  $\lambda$ 2344 in the arithmetic mean composite spectra of subsamples. Sample numbers are given in the rightmost panels. Selection criteria for the samples (as given in Table 1) are briefly described below for ease in comprehension. The pairings are, with the samples plotted and labeled in red given first, SY06, No. 1: full samples of intervening and associated absorbers; Nos. 2, 3:  $i$  magnitude  $<$  and  $\geq 18.74$ ; Nos. 4, 5:  $W_{\text{Mg II}} <$  and  $\geq 1.35 \text{ \AA}$ ; Nos. 6, 7:  $\beta <$  and  $\geq 0$ ; Nos. 10, 11: radio-detected and undetected QSOs.

shows that the emission-line profiles in the QSOs with associated absorbers and QSOs without associated absorbers are, on average, similar in shape. This possibly also indicates that the emission seen in the extinction curves of Figure 5 is not real and is an effect of the difference in the emission redshifts of the absorber and nonabsorber QSOs. We cannot, however, completely rule out emission from the absorbers.<sup>10</sup>

About 28% of the QSOs in sample 1 also have other intervening absorption systems in their spectra. These, in principle, could contribute to the values of  $E(B-V)$  determined here. The

<sup>10</sup> The extended emission regions (EELR) as seen in [O II] and other lines discussed in the literature are mainly  $< 30$  kpc in size. The  $3''$  fibers of the SDSS spectroscopic survey include that region, for all QSOs discussed here. Similar regions in radio galaxies show emission in [C III] and Mg II (McCarthy 1993), which do not show up in the same strengths in standard H II regions (Garnett et al. 1999). Hamann et al. (2001) compute the emission line strengths of Mg II EELR of 3C 191, predicting an equivalent width relative to the local QSO continuum of  $4 \text{ \AA}$  (1/3 of that for [O II]). The combined equivalent width of the Mg II absorption lines in Fig. 5 is  $2.6 \text{ \AA}$ , and the emission would be broader and more washed out. Haiman & Rees (2001) predict that infalling material could produce detectable Ly $\alpha$  emission from such core regions. Evidently, detection of emission from the EELR should be possible in SDSS composite spectra, if the intrinsic QSO emission can be modeled precisely enough.

effect is likely to be small, in view of the results of Y06, which showed that intervening systems with  $W_{\text{Mg II}}$  smaller than  $1.53 \text{ \AA}$  do not produce significant reddening, and far outnumber the systems with stronger Mg II absorption that do produce reddening. However, to evaluate the effect of these intervening systems, we constructed composites for the subsample of 298 associated systems (from our sample 1) which had no other absorption systems in their spectrum. The  $E(B-V)$  for this subsample is  $0.029 \pm 0.003$ , which is the same as that of sample 1, to within the errors. We thus conclude that the other systems in 117 QSOs in our sample 1 are too weak to affect the value of  $E(B-V)$  due to associated systems determined here.

The extinction for the full sample [No. 1;  $E(B-V) = 0.026 \pm 0.004$ ] is twice that obtained for the intervening sample [SY06;  $E(B-V) = 0.013$ ], indicating a higher amount of dust in the associated systems.<sup>11</sup> This could partly be due to the following

<sup>11</sup> This qualitative statement is conservative. That is, there is an evident discontinuity near  $3650 \text{ \AA}$  in the composite spectra of the QSOs with Mg II associated absorbers (Fig. 5, top). We assume that the true extinction is continuous and that the noted discontinuity is a feature intrinsic to the QSO spectra or is an artifact of the reductions. This is reflected in our normalization at  $3000 \text{ \AA}$ , which gives a lower limit to the color excess inferred.

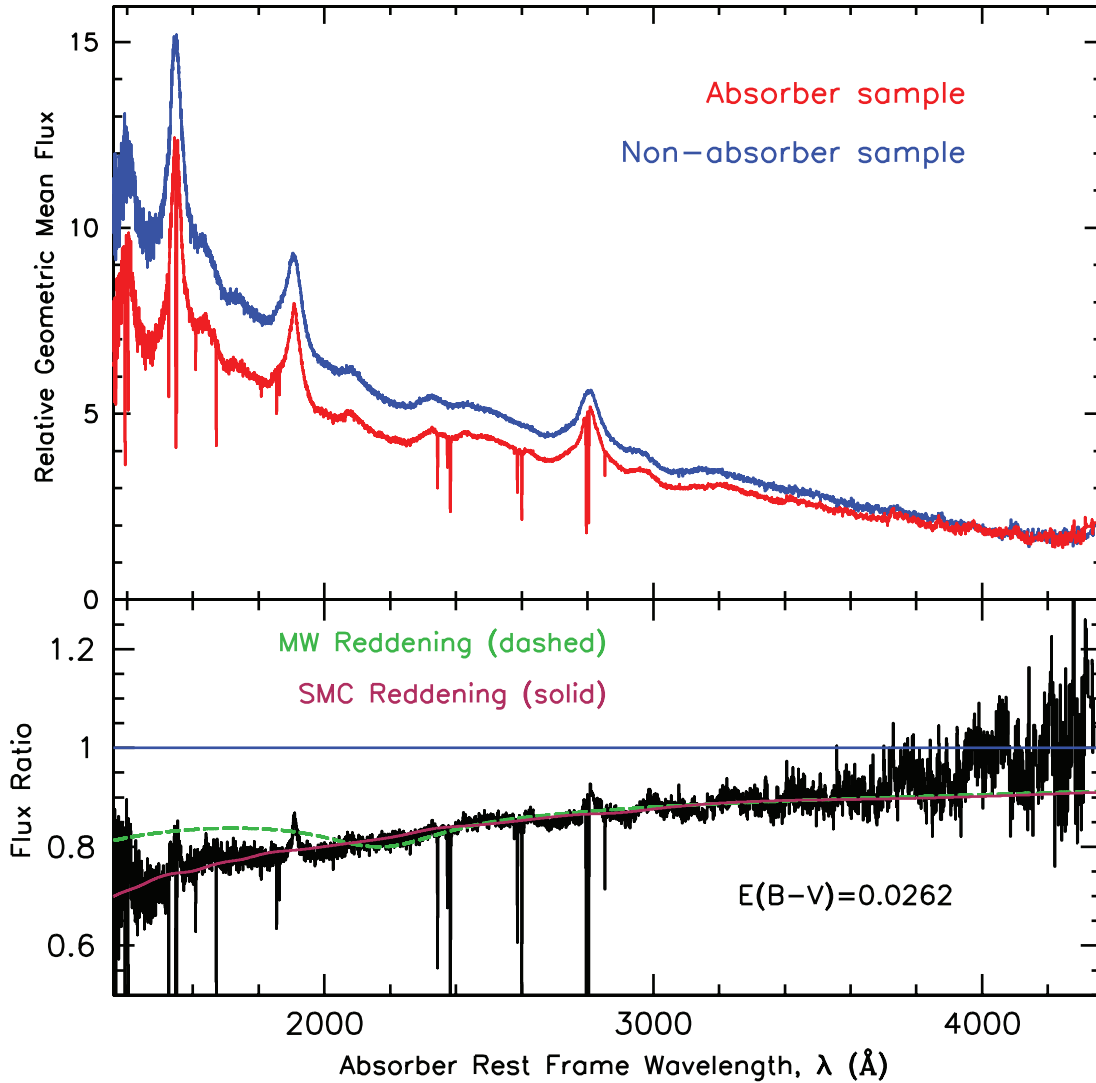


FIG. 5.— *Top*: Geometric mean composite spectrum of the QSOs in sample 1, in the absorber rest frames (*red*), and that of the corresponding nonabsorbers (*blue*). Note that emission lines do appear in the absorber rest-frame composite spectrum due to the small difference in emission and absorption redshifts of the QSOs in the sample of associated systems. The absorption lines in the red spectra are obvious. See text for a discussion of the normalization of the plots. *Bottom*: Ratio of the two spectra along with the best-fit SMC extinction curve in red. The derived absorber rest-frame  $E(B-V)$  value is given. The MW extinction curve for the derived SMC  $E(B-V)$  value is shown in green.

reason. As noted in the last subsection, the ionization level is higher in the associated systems. Thus, by choosing systems with  $W_{\text{Mg II}} > 0.3$  Å, we have possibly chosen associated systems with a higher total Mg column (that is, including all ionization states) and thus higher total hydrogen column, and therefore a higher dust column as compared to those in the intervening systems. We note that the average  $W_{\text{Mg II}}$  in the intervening systems (1.73 Å) is higher than that in the associated systems (1.54 Å). This could be due to the ionization effect mentioned above. It is, however, not clear if the higher  $E(B-V)$  in the associated systems is due to this effect alone. It is possible that the associated systems have higher a dust-to-gas ratio. It is also possible that part of the reddening is caused by the dust intrinsic to the QSO, but not containing Mg II (because of ionization?). As shown in the next subsection, the reddening is strongly dependent on the radio properties of the QSOs. We return to these points below.

The extinction in the subsample of faint QSOs (No. 3) is somewhat higher than that in the subsample of bright QSOs (No. 2). The average  $W_{\text{Mg II}}$  for the fainter subsample is higher (1.70 Å) than that for the brighter subsample (1.37 Å). This

possibly indicates that the fainter QSOs are fainter because of the higher dust content of the absorbers lying in front of them. In the subsample of systems with  $W_{\text{Mg II}} > 1.35$  Å (No. 5) it is close to 2 times that in the subsample of systems with  $W_{\text{Mg II}} < 1.35$  Å (No. 4). Surprisingly, the value of  $E(B-V)$  is 1.5 times higher in associated systems with negative  $\beta$  (No. 6) than those with positive  $\beta$  (No. 7). Note that both of these subsamples have similar values of  $W_{\text{Mg II}}$ . As noted in the previous subsection, the ionization seems to be higher in subsample 6 than in subsample 7. The higher amount of dust may thus indicate a higher amount (by a factor  $\sim 1.5$ ) of total hydrogen (neutral plus ionized) in the latter. A similar dependence of  $E(B-V)$  on  $\beta$  is observed if we divide the positive  $\beta$  subsample (No. 7) into two halves at the median value of 0.004. The lower  $\beta$  subsample has  $E(B-V)$ , which is higher than that of the high  $\beta$  subsample. The effect is also seen in subsamples 13 and 14. Thus, the  $\beta$  values seem to be an indicator of the state of ionization of the absorbers and of the amount of reddening. Similar effects have been noted by Baker et al. (2002) and V03 using less quantitative means. The effect found here is much more subtle than that claimed by Baker et al.

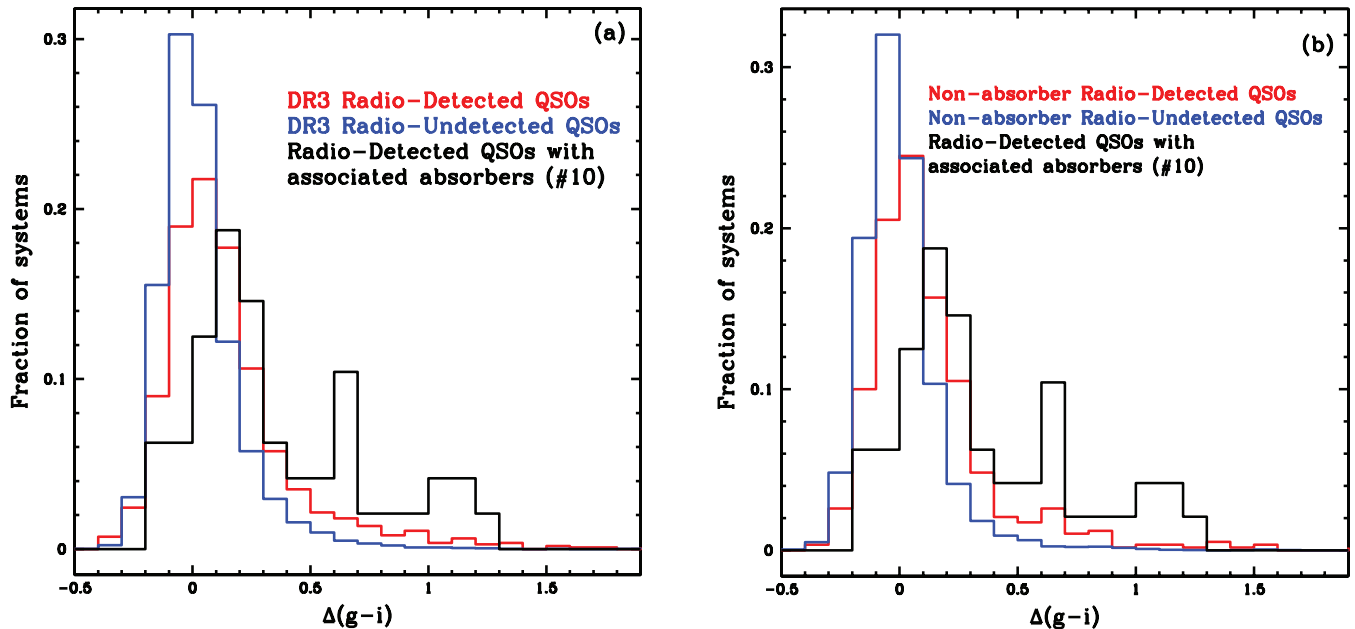


Fig. 6.— (a) Distribution of  $\Delta(g-i)$  in SDSS DR3 QSOs with  $1.0 < z_{\text{em}} < 1.96$ , having (i) nonzero FIRST flux (red) and (ii) nondetection in the FIRST survey (blue). Also shown is the distribution for FIRST radio-detected QSOs in our subsample (No. 10) of associated systems (black). (b) Distribution of  $\Delta(g-i)$  in SDSS DR3 QSOs with  $1.0 < z_{\text{em}} < 1.96$ , confirmed by the present study as having no absorption systems in their spectra and having (i) nonzero FIRST flux (red) and (ii) nondetection in the FIRST survey (blue). Also shown is the distribution for FIRST radio-detected QSOs in our subsample (No. 10) of associated systems.

(2002). The effect of radio properties of the QSOs on the extinction is discussed in the next subsection.

### 3.4. Dependence on Radio Properties of QSOs

In our sample of the associated systems, 48 QSOs have nonzero FIRST flux (the RD subsample, No. 10) while 318 QSOs have nondetection in the FIRST survey (the RUD subsample, No. 11); the rest have not been observed by the FIRST survey. (Hereafter, we drop reference to the FIRST survey, which is implied when we refer to radio sources.) In the SDSS DR3, the number of QSOs with  $z_{\text{em}}$  between 1 and 1.96 is 23,914, in all of which we could have seen associated Mg II absorbers if present. Of these, 1728 are RD and 19,056 are RUD (the rest have not been observed by the FIRST survey). As the selection criterion for the RD and RUD subsamples (as described in § 2.1) were identical and because the average observed  $i$  magnitudes (18.60 and 18.63 for the RD and RUD subsamples, respectively), the average absolute  $i$  magnitudes ( $-26.35$  and  $-26.52$  for the RD and RUD subsamples, respectively), and  $z_{\text{abs}}$  (1.39 and 1.5 for the RD and RUD subsamples respectively) of the two subsamples are almost equal, no other biases are present, and we can compare the frequency of occurrence of these systems. Thus, the incidence of associated absorbers with  $W_{\text{Mg II}} > 0.3 \text{ \AA}$  in RD QSOs is 2.8%, while that in RUD QSOs is 1.7%. RD QSOs are thus 1.7 times more likely to have associated absorption than the RUD QSOs. Assuming binomial statistics, the probability of getting such a large difference in the incidence of associated systems between the two subsamples is less than 1%.

#### 3.4.1. Intrinsic Redness of Radio-Detected QSOs

As can be seen from Table 1, the reddening in the RD QSOs with associated Mg II systems is 5 times higher than that in the RUD QSOs. As noted in § 1, associated C IV absorption may occur preferentially in steep-spectrum radio sources. If, as is often assumed (see § 1), such sources are viewed in the edge-on position, it is possible that the material in the accretion disk/torus

(unrelated to the absorption systems) may be causing part or even most of the observed reddening in the radio-loud QSOs. The “redness” of radio QSOs has been noted earlier (e.g., Brotherton et al. 2001; Baker et al. 2002; Ivezić et al. 2002).

To investigate this, we have, in Figure 6a, plotted histograms of  $\Delta(g-i)$  of all RD (red lines) and RUD (blue lines) QSOs with  $1.0 < z_{\text{em}} < 1.96$  (which is the emission redshift range of our sample of associated absorbers) in the DR3 catalog (Schneider et al. 2005). It can be seen that the RD QSOs have a higher fraction of red QSOs as compared to that in RUD sample (the red histogram is shifted to the right). As many of the QSOs in the DR3 RD and RUD subsamples may have absorption systems, we have in Figure 6b, plotted similar histograms for RD and RUD subsamples of nonabsorber DR3 QSOs having  $z_{\text{em}}$  between 1 and 1.96. There are 580 RD nonabsorber QSOs (red lines) in this redshift range, while there are 6786 RUD nonabsorber QSOs (blue lines). According to Y06, unreddened, unabsorbed QSOs have  $-0.2 < \Delta(g-i) < +0.2$ , consistent with the RUD nonabsorber QSOs plotted in Figure 6b. The RD nonabsorber QSOs have a much larger fraction of red QSOs than the RUD nonabsorber sample. Thus, we have definite evidence of RD QSOs being intrinsically redder than the RUD QSOs.

In order to quantify the intrinsic redness of the RD nonabsorber QSOs, we constructed a composite spectrum of 250 RD nonabsorber QSOs in the QSO rest frame and compared it with similar composite spectrum of matching (in  $i$  magnitude and  $z_{\text{em}}$ ) 250 RUD nonabsorber QSOs. The KS test shows that the  $i$  magnitude and  $z_{\text{em}}$  values in the two subsamples are drawn from the same distributions. The composite spectrum of the RD nonabsorber QSOs is redder than that of RUD nonabsorber QSOs. To avoid effects due to the selection of matching nonabsorber subsamples, instead of determining the absolute  $E(B-V)$  values for these subsamples, we directly determine relative  $E(B-V)$  values between these two subsamples by fitting an SMC extinction curve to the ratio of their composite spectra. This gives the relative  $E(B-V) = 0.036 \pm 0.0001$  as the intrinsic average color excess

TABLE 4  
RELATIVE  $E(B-V)$  VALUES FOR SEVERAL SUBSAMPLES

Sample A	Sample B	Description of Comparison	$E(B-V)^a$
250 RD, nonabsorber QSOs.....	250 RUD, nonabsorber QSOs	Nonabsorber: RD/RUD	$0.036 \pm 0.0001$
No. 1 .....	SY06	Associated/intervening	$0.027 \pm 0.0001$
No. 10 .....	No. 11	Associated: RD/RUD	$0.074 \pm 0.0002$
SY06RD.....	SY06RUD	Intervening: RD/RUD	$0.033 \pm 0.0001$
No. 10 .....	SY06RD	RD: associated/intervening	$0.062 \pm 0.0001$
No. 11 .....	SY06RUD	RUD: associated/intervening	$0.018 \pm 0.001$
No. 10 with $W_{\text{Mg II}} \geq 1.58$ .....	No. 10 with $W_{\text{Mg II}} < 1.58$	Associated, RD: strong Mg II/weak Mg II	$0.092 \pm 0.003$
No. 10 with $1.22 \leq W_{\text{Mg II}} \leq 2.1$ .....	No. 10 with $W_{\text{Mg II}} < 1.22$	Associated, RD: intermediate Mg II/weak Mg II	$0.074 \pm 0.001$
No. 10 with $W_{\text{Mg II}} \geq 2.1$ .....	No. 10 with $1.22 \leq W_{\text{Mg II}} < 2.1$	Associated, RD: strong Mg II/intermediate Mg II	$0.053 \pm 0.001$
Color-selected QSOs from subsample No. 10.....	Color-selected QSOs from SY06RD	RD, color-selected: associated/intervening	$0.048 \pm 0.0001$

<sup>a</sup> Relative  $E(B-V)$  of sample A with respect to sample B, obtained by fitting an SMC extinction curve to the ratio of composite spectra for subsample A and B. To estimate the uncertainty of the  $E(B-V)$  value, 10 simulated extinction curves were generated by adding noise to the original extinction curve, consistent with the error array. The values of  $E(B-V)$  were calculated for each of 10 simulated extinction curves, and the rms dispersion of the values is taken as the estimate of the  $E(B-V)$  value uncertainty.

in RD QSOs over RUD QSOs. This value and values of relative  $E(B-V)$  among several other subsamples are given in Table 4.

#### 3.4.2. Dependence of Extinction Properties of Associated Absorbers on the Radio Properties of QSOs

To test whether the higher  $E(B-V)$  in RD QSOs is solely because of the intrinsic dust in these QSOs or if the associated absorbers in these QSOs also have higher dust content as compared to the rest of the associated absorbers, in Figures 6a and 6b we have plotted the histograms of  $\Delta(g-i)$  (black lines) for subsample 10. It is clear that the RD QSOs with associated absorbers have a higher fraction of red QSOs than the RD nonabsorbers (the black histograms extend more to the right). Thus, the RD QSOs with associated absorbers are more likely to be reddened than those without such absorbers. While 56% of RD QSOs with associated absorbers have  $\Delta(g-i) > 0.2$ , the numbers for the RD and RUD nonabsorber QSOs (with  $z_{\text{em}}$  between 1 and 1.96) are 26% and 8%, respectively. The three numbers for  $\Delta(g-i) > 0.5$  are 31%, 9%, and 1.6%, respectively. Evidently, studies of extinction in radio QSOs must consider whether associated absorbers are present or not, especially in individual cases.

In order to quantify this result further, we compiled a matching sample of QSOs (for the absorber QSOs in subsample 10) from among the RD nonabsorber QSOs. The resulting  $E(B-V)$  was found to be  $0.062 \pm 0.007$  (see footnote d in Table 1), smaller than the  $E(B-V)$  of subsample 10 in Table 1 by a factor of only 1.4, showing that although the RD nonabsorber QSOs are redder than the RUD nonabsorber QSOs, a significant fraction of the reddening in our subsample of RD QSOs is caused by the dust in the associated absorbers.

As noted in § 3.2, the average  $W_{\text{Mg II}}$  of the RD subsample (No. 10, 1.9 Å) with associated Mg II absorbers is higher than that of the full sample (No. 1, 1.54 Å). Although higher  $W_{\text{Mg II}}$  is likely to be indicative of a larger velocity dispersion of Mg II lines, a correlation between  $E(B-V)$  and  $W_{\text{Mg II}}$  has been noticed by Y06, and is also seen in our sample (see subsamples 4 and 5 in Table 1). Thus, the higher  $W_{\text{Mg II}}$  of the RD subsample could be partially responsible for the higher  $E(B-V)$ . However, we note that the  $E(B-V)$  for the RD subsample (No. 10) is much higher than for the subsample (No. 5) of strong systems, for which the average  $W_{\text{Mg II}}$  is 2.23 Å but  $E(B-V)$  is only  $0.034 \pm 0.003$ . Thus, the somewhat higher average  $W_{\text{Mg II}}$  for the RD subsample

compared to the RUD subsample is not the sole reason for the high value of  $E(B-V)$ , which is definitely related to the QSOs being RD.

If a large part of the excess extinction observed in RD QSOs (over RUD QSOs) is generated in the associated absorbers, then the  $E(B-V)$  values in these QSOs will depend on the absorber properties. In order to investigate this issue, we divided the subsample of RD QSOs (No. 10) into two parts, at the median value of  $W_{\text{Mg II}}$  of 1.58 Å. The relative  $E(B-V)$  value of the high  $W_{\text{Mg II}}$  subsample with respect to the low  $W_{\text{Mg II}}$  subsample (obtained by fitting an SMC extinction curve to the ratio of the composite spectra of the two subsamples) is  $0.092 \pm 0.003$ . Division into three equal parts based on  $W_{\text{Mg II}}$  ( $W_{\text{Mg II}} < 1.22$ ,  $1.22 < W_{\text{Mg II}} < 2.1$ , and  $W_{\text{Mg II}} > 2.1$  Å) gives relative  $E(B-V)$  (obtained as explained above) =  $0.074 \pm 0.001$  and  $0.053 \pm 0.001$  for the two pairs of neighboring subsamples (the higher  $W_{\text{Mg II}}$  subsamples being redder). The values of relative  $E(B-V)$  are given in Table 4. It is clear that the  $E(B-V)$  is correlated with  $W_{\text{Mg II}}$ . The Spearman rank test to determine the presence of a correlation between  $W_{\text{Mg II}}$  and  $\Delta(g-i)$  gives  $R_s = 0.463$  and the probability of chance correlation to be 0.001. Thus, it is very clear that the higher reddening in the RD QSOs with associated absorbers is strongly correlated with the strength of Mg II absorption lines, and should therefore be due to the dust present in the absorbers. The fact that RD QSOs are intrinsically redder, evidently harboring more dust in their associated systems (as compared to that in the systems associated with the RUD QSOs) may indicate that the absorbing material is similar to that in the QSO, and may thus be intrinsic to the QSO. We do not, however, find any evidence of enhanced abundances in the composite spectra (as in Fig. 3), as discussed in § 3.5 below.

#### 3.4.3. Comparison with the Intervening Sample

A significant contribution to the  $E(B-V)$  value for the full sample (No. 1) must come from the RD QSOs. For 49 objects in that sample, no radio observations are available. Some of these could also have significant radio flux. The RUD subsample (No. 11) has  $E(B-V)$  of  $0.016 \pm 0.004$ . The QSOs in the matching nonabsorber samples for these do have some RD QSOs, so the value of  $E(B-V) = 0.016$  is a lower limit. Restricting the nonabsorber sample to RUD QSOs, we get  $E(B-V) = 0.018 \pm 0.0007$  (see Table 1 footnote e). We have to compare these values with  $E(B-V)$  values for similarly selected subsamples of

the intervening systems (SY06). In SY06, 41 systems have been detected by the FIRST survey, while 614 are RUD; the remaining 129 have not been observed by the FIRST survey. The relative  $E(B-V)$  values between the RD and RUD intervening and associated subsamples are given in Table 4. We find that the RD associated systems have a relative  $E(B-V)$  of  $0.062 \pm 0.0001$  with respect to the RD intervening systems. The RUD associated systems have a relative  $E(B-V)$  of  $0.018 \pm 0.001$  with respect to the RUD intervening systems. Thus, the RD QSOs with associated absorbers are definitely more reddened than the RD QSOs with intervening absorbers. The RUD QSOs with associated absorbers are also more reddened than the RUD QSOs with intervening absorbers. Thus, on the whole, the associated absorbers are dustier than the intervening absorbers.

#### 3.4.4. SDSS Color-Selected Radio-Detected QSOs

As noted in § 2.1, SDSS QSOs are mostly color selected, but some QSOs (particularly those below  $i$  magnitude of 19.1) are selected because they are *ROSAT* or FIRST sources. Such sources may be redder than the average because they may not satisfy the SDSS color-selection criteria, but instead have colors consistent with the stellar locus. It is possible that the presence of such sources in the RD sample (No. 10) may be responsible for the excess reddening in this subsample. Ten sources in subsample No. 10 are not color-selected, while two of the RD QSOs in SY06 are not color-selected. The relative  $E(B-V)$  of the subsample of color-selected RD QSOs with associated systems with respect to the color-selected RD QSOs with intervening systems (see Table 4) is  $0.048 \pm 0.0001$  (compared to 0.062 when the non-color-selected QSOs are included). Thus, the color-selected RD QSOs with associated absorbers are significantly redder than the color-selected RD QSOs with intervening absorbers.

#### 3.4.5. Radio Morphology

As noted above, the presence of associated absorbers in radio QSOs may be correlated to the morphology and radio spectral slope of these QSOs. Outflows from QSOs (e.g., jets or accretion disk winds) can give rise to associated systems (e.g., Richards et al. 2001; Misawa et al. 2007). Models using beamed radio jet emission have been proposed to unify flat-spectrum radio quasars and steep-spectrum radio galaxies (e.g., Orr & Browne 1982; Padovani & Urry 1992). On average, a flat-spectrum quasar is thought to be viewed closer to the jet axis than a steep-spectrum quasar. Here we examine the radio morphologies and spectral indices of quasars with and without associated absorption, with the hope of understanding the connection between the direction of motion of the outflow (e.g., polar or equatorial) and the absorber properties.

To study the radio morphology of quasars in our subsamples, we proceeded as follows. For each of the 48 RD quasars with associated absorbers (sample 10), we searched for sources detected in the FIRST image within  $1.0'$  of the quasar's optical (SDSS) coordinates. (At  $1 < z < 2$ , an angular separation of  $1'$  corresponds to about 500 kpc for the concordance cosmology.) First, we visually examined the morphologies in the FIRST images. If the source was clearly resolved as a multicomponent source (i.e., at least 1 distinct source besides the core was found within about  $30''$ ), then we considered the source a lobe ("L") source. If a single source, without a counterpart on the other side, was found between  $30''$  and  $60''$  from the core, then it is likely not related to the quasar, and we treated the quasar as a core ("C") source, rather than a lobe source. For the objects with no other source found within  $60''$  of the core, we quantified the morphology using the procedures of Richards et al. (2001)

and Ivezić et al. (2002). For each source, the FIRST catalog lists the peak and integrated flux densities. Using these, we determined a dimensionless measure of concentration of radio emission,

$$\theta = (F_{\text{int}}/F_{\text{peak}})^{1/2}. \quad (1)$$

We classified the single sources with  $\log \theta^2 \leq 0.1$  as core-dominated ("C") and those with  $\log \theta^2 > 0.1$  as partially core-dominated ("PC") sources. (In a few C cases, the values of  $\log \theta^2$  are slightly negative due to the uncertainties in the FIRST flux measurements.) Finally, we checked that the above quantitative divisions between C and PC are consistent with the contour maps of the FIRST images. (For only one C source in the absorber sample, large-scale artifacts in the FIRST data give rise to  $\log \theta^2 > 0.1$ .) With these definitions, the 48 quasars in sample 10 consist of 26 C, 8 PC, and 14 L sources. Thus, 46% of the sources in the absorber sample are spatially resolved (PC or L type).

To understand how far these fractions relate to the existence of an associated absorber along the sight line, we repeated the above procedure for the matching 48 RD quasars with no absorbers. Of these 48 quasars, 31 are C sources, 6 are PC sources, and 11 are L sources. Thus, 35% of the sources in the non-absorber sample are spatially resolved. There is thus a slight excess of spatially resolved sources in the absorber sample compared to the nonabsorber sample. Using binomial statistics, the probability of finding a fraction of 46% or more resolved sources in the absorber RD sample if the true fraction is only 35% is about 0.08. Thus, the difference between the samples is not highly significant. To confirm such an excess at the 1% level would require a sample size of about 100 objects, which should be possible to construct from the SDSS DR5 QSO data set.

We constructed absorber rest-frame composite spectra of the 26 C QSOs and of the 14 L QSOs. As the line of sight to the L QSOs is expected to pass near or through the accretion disk, these QSOs are expected to be more reddened. However, we find that the C composite is redder than the L composite, the relative  $E(B-V)$  being 0.042. This could very well be a small-sample effect, and it will be very interesting to repeat this for bigger samples.

It is not possible to determine radio spectral indices for all of the quasars in the RD absorber and nonabsorber samples, since flux densities at wavelengths other than 20 cm are not available for most of them. Of the 48 RD quasars with associated absorbers, only 15 have measurements at other wavelengths (14 from the Green Bank [GB] 6 cm catalog [White & Becker 1992], and one at 80 cm). Using these along with the 20 cm FIRST measurements, we calculated the spectral indices. (In a few cases, the spectral index based on the GB and FIRST measurements is somewhat different from that listed in White & Becker [1992], which probably results from different resolutions of the two surveys and possible variability between the two epochs of observation.) In any case, taking the spectral index  $\alpha_{\text{int}}$  thus calculated using integrated flux densities, we classified objects as flat-spectrum ("F") if  $|\alpha_{\text{int}}| \leq 0.4$ , and steep-spectrum ("S") otherwise. Of the 15 quasars in the absorber sample where we could determine  $\alpha_{\text{int}}$ , eight are F sources. Of the seven steep-spectrum sources, five have  $\log \theta^2 \leq 0.10$  and are thus likely to be compact. This suggests that these associated absorbers are associated with outflow material located close to the polar direction. In the nonabsorber sample, 6 cm fluxes are available for seven quasars, of which four are steep-spectrum sources (including one compact steep-spectrum source).

Thus, compact steep-spectrum sources may be more common in cases with associated absorbers.

Overall, some fraction of the associated absorbers appear to arise in material along the polar axis, while others arise in material away from the polar axis. Larger samples are needed to systematically study correlations among the absorber properties and outflow orientation and line-of-sight velocity.

### 3.5. Abundances

There seems to be wide agreement that the abundances in the broad emission line regions are supersolar (Ferland et al. 1996; Hamann & Ferland 1999; Hamann et al. 2002; Baldwin et al. 2003; Nagao et al. 2006; Dhanda et al. 2007), and the same is true for the narrow-line regions of Seyfert 2 galaxies (Groves et al. 2006). There are a number of instances of suspected supersolar abundances in associated absorbers (D’Odorico et al. 2004; Hamann 1997; Petitjean et al. 1994; Tripp et al. 1996). Fu & Stockton (2006) discuss the contamination of the broad-line region and EELR by mergers with galaxies with subsolar abundances.

It can be seen from Table 3 that for the weakest lines of dominant ions of Mn (three lines near 2600 Å), Fe ( $\lambda\lambda 2260, 2249$ ), Cr (three lines near 2062 Å), and Zn ( $\lambda\lambda 2026, 2062$ ), the ratios of lines of each species indicate that the weakest lines are on the linear portion of the curve of growth, independent of the Doppler widths or the width or saturation of the stronger lines. We assume that Si II  $\lambda 1808$  is on the linear portion of the curve of growth. (Note that the relative strengths of  $\lambda 1808$  and  $\lambda 1526$  indicate that the Doppler width, in this case related to the spread of components, is probably somewhat higher in sample 1 than in sample SY06, making our assumption conservative.) Then, the equivalent widths of the weakest lines of these species are proportional to the column densities. We find that the equivalent widths of the weakest lines of these ions are weaker in sample 1 (associated system average) than the lines of the intervening averages (SY06): the ratios (sample 1 divided by SY06) are 0.8, <0.8, 0.9, 1, and <0.8 for Si II, Cr II, Mn II, Fe II, and Zn II, respectively. The value for Zn II accounts for the fact that we cannot deblend the Cr II 2062 line in sample 1 as we could in the SY06 sample. On the other hand, the same ratio for Ni II might be as high as 5 for the weakest line, but of order 1.4 for two other lines of comparable strength.

The extinction is twice as high in sample 1 [ $E(B - V) = 0.026$ ] as in SY06 (0.013). If the ratio of  $E(B - V)$  to the  $N_{\text{H I}}$  value is the same in associated and intervening systems, then the abundances in sample 1 are slightly less than in SY06. There is no evidence that the associated systems containing Mg II have greatly enhanced abundances that would indicate an association of the associated systems with the gas from the QSO emission-line region.

Of course, the dust might be different in the two types of systems, but the extinction curves are of the same general shape. There could be ionization corrections that would modify this indication of abundances; high-resolution observations and analysis with CLOUDY, as shown, for instance, by Meiring et al. (2007), will be required to search for a stronger statement about the abundances. Higher resolution is needed to resolve the individual components in the systems and to resolve the contrary indication from the one result for Ni II.

Thus, from our results there is no strong effect averaged over 415 associated absorbers studied here that would indicate a relation of those absorbers to gas originating in the broad-line regions.

### 3.6. Location and Nature of the Absorbers

We find several suggestions for the origin of the associated absorbers. First, the ionization effects in Si IV, C IV, and Mg II and

their dependence on  $\beta$  indicate that lower  $\beta$  systems are closer to the QSO. The various suggestions discussed above that place some of the associated systems in the EELR, and the confirmed existence of negative  $\beta$  systems, may be related to the large widths (400 km s<sup>-1</sup>; Fu & Stockton 2006) and bigger shifts (1800 to -600 km s<sup>-1</sup>) of emission lines in the EELR (Christensen et al. 2006). While these do not quite add up to the negative  $\beta$  values of 0.004 found here, the sample of EELR is small; a larger sample may show that a wider range exists, comparable to that seen in our Mg II absorbers. An extensive study of the associated systems found here is in order, at high resolution, to determine abundances and populations of fine-structure excited states.

We also note the anomaly in Mg I absorption line strengths mentioned earlier. Hamann et al. (2001) found relatively strong Mg I lines in the associated gas in 3C 191 and drew an analogy to the strong Na I absorption in superwinds that seem to have cool clumps within them (Heckman et al. 2000), which is most evident when the galaxies are seen pole-on and have moderately high (600–800 km s<sup>-1</sup>) ejection velocities. Perhaps, with the same conditions but for a luminous QSO within tens of kpc, the temperature is tuned to allow a higher recombination rate for Mg I owing to dielectronic recombination (York & Kinahan 1979), and the density is high enough to make Mg I particularly strong. Hamann et al. (2001) note that we have few spectroscopic diagnostics and few cases where we can determine multiple diagnostics in associated systems: for example, appropriate fine-structure lines work only for gas densities of a few hundred, for first ions but not for second ions; also, there are not many neutral species detectable to establish photoionization rates, which might shed light on the distances from the QSO. Likewise, a discrete and even higher density range is accessible using the excited Fe II lines (Wampler et al. 1995). There may be a wide range of conditions, but only a few that we can pick out and analyze because of the unavoidable selection effects associated with atomic or ionic parameters. Eventually, high-resolution, high-S/N observations may reveal subtle examples of regions with a wider range of conditions, and provide more insight into the likely origin of individual systems.

How can we tell if an apparently low  $z$  (compared to  $z_{\text{em}}$ ) absorber is intervening or is ejected from the background QSO at high velocity? Two attributes seem to distinguish the associated absorbers ( $\beta < 0.01$ ) studied here from the intervening absorbers ( $\beta > 0.01$ ): the higher ionization (specifically, the higher ratio of  $W_{\text{C IV}}$  and probably  $W_{\text{Si IV}}$  to  $W_{\text{Mg II}}$ , on average), and the higher ratio of  $E(B - V)$  to  $W_{\text{Mg II}}$  in the associated systems. The latter difference would be hard to distinguish in the case of an individual absorber, because of the range of intrinsic energy distributions of QSOs at a given redshift (Vanden Berk et al. 2001; Richards et al. 2002a; Richards 2006). Whether the former can be a discriminant in individual cases remains to be seen. In view of the much higher  $E(B - V)$  values for the associated systems in RD QSOs, we suggest that these are possibly intrinsic to the QSOs. Ganguly et al. (2001) and V03 assumed that only C IV systems (no low ions) were nonintervening systems. That appears from our study not to be true.

A third possible distinguishing characteristic would be the abundances, which are possibly higher in associated systems in the sense of being close to the QSO, whatever the inferred velocity of ejection, if the gas comes from the region of enhanced emission-line abundances of the AGN, as noted in § 3.5. On the other hand, on average, there is little evidence that the associated Mg II absorbers have enhanced abundances. In light of the recent detection of intervening absorbers with supersolar abundances (e.g., Khare et al. 2004; Peroux et al. 2006; Meiring et al. 2006),

this question cannot be answered until there is a significant search for the intervening galaxies near supposedly intervening QSO absorption-line systems. If no galaxies are found near some high-metallicity QSO absorption-line systems, the possibility of high-velocity ejecta from the central region of the AGN may need to be entertained.

The other well-known indicators of intrinsic absorbers are the nonunity covering factor and short time variability of the absorption lines.<sup>12</sup> The former does not appear to be widespread, as the effect does not appear in our samples (but see Misawa et al. [2007] for a significant effect in weaker lines at higher redshift than in our sample). Apparently, only spectra of individual objects, with high S/N, can be used to discern the effect, which may be rare.

#### 4. SELECTION EFFECTS IN OUR STUDY

The results presented here relating to correlations with  $\beta$  depend on the correctness of our values of  $\beta$ . Richards et al. (2002b) and Richards (2006) summarized many years of research on the origin of the shifts between C IV and Mg II emission lines in the same QSO. They argue that the shifts arise from measuring the centroid of C IV emission lines that are attenuated on the redward edge of the C IV profile, shifting the centroid blueward. Furthermore, the degree of this blueshift is more extreme in sources that have bluer QSO continua, are not radio sources, and are not X-ray sources. These same properties apply to the sources that have BAL systems, that is, highly blueshifted absorption systems with much broader lines than the  $<500 \text{ km s}^{-1}$  wide lines selected in our QSOALS catalog. Of course, since the physics of the associated QSOALS and the BALs is equally uncertain, there may be no sharp distinction between the origin of the two types of absorption lines. At any rate, the origin and ionization of the associated systems and the origin of the optical depth effects might be related, imposing a correlation between  $\beta$  and ionization from some source other than what we discuss above.

We have shown that the redshifts derived using an empirical SDSS correction procedure agree with the redshifts (hence, derived  $\beta$  values for absorbers) found from the narrow [O II] lines, which should give the systemic velocity of the QSO host galaxy. Thus, the effects noted above may not be very important. However, that line is not always available, and we depend on redshifts from broad lines in particular cases.

Other subtle correlations between absorption lines and the background QSOs might affect the present study. (1) The negative velocity and positive velocity apparent motions of the associated absorbers may not be physically related in a continuous fashion; the negative and positive  $\beta$  systems might have a different physical origin. (2) With larger samples and further sharpening of the definitions of “associated,” “intervening,” and “ejected,” it may be possible to further refine the selection of “associated” systems. It may be that in our sample we have mixed in some true intervening systems that are nonetheless near the QSO, or that some ejected systems, having higher velocities than  $3000 \text{ km s}^{-1}$ , have been included in our “intervening” sample. Richards et al. (1999) suggest that one may have to pick a pure intervening sample from systems that have  $\beta > 0.1$  to be free of ejected material. (3) Our use of the absolute  $i$  mag-

nitude to construct matched pairs may not completely control for intrinsic variations in the QSO continuum among absorber and nonabsorber samples. X-ray, radio, and infrared luminosities may be needed to be matched for a thorough removal of such effects. Measurements of these are often unavailable, or are only available to flux limits of surveys that could be inadequate for the task. (The best available X-ray and near-IR survey data matched to the SDSS data are described by Anderson et al. 2007 and Ivezić et al. 2002).

Finally, we caution that the trends in the state of ionization of the absorbers, as noted by us, need to be confirmed by higher resolution observations, as line saturation is likely to be significant for Mg II lines.

#### 5. CONCLUSIONS

We have studied a sample of 415 intermediate-redshift, Mg II associated systems in the spectra of SDSS QSOs. Our main conclusions are as follows.

1. There is definite evidence of dust extinction in the associated systems. The average extinction is 2 times that found in a sample of similarly selected intervening systems. This larger extinction could be attributed to higher average  $N_{\text{H I}} + N_{\text{H II}}$  in associated compared to intervening systems, or to differences in the dust-to-gas ratio.

2. There is no evidence for the 2175 Å bump in the extinction curves of the associated absorbers.

3. The extinction curve for these absorbers is similar to that of the SMC, which has also been found to be the case for intervening absorbers.

4. Associated absorbers are in a higher state of ionization than the intervening absorbers.

5. In the relative velocity range  $0.01 > \beta > -0.004$  studied, the ionization conditions and the total extinction in the associated systems is a function of their apparent relative velocity with respect to the QSO, systems with lower relative velocity being more ionized and more highly reddened.

6. There is no obvious evidence for higher abundances in the associated systems than those in the intervening systems.

7. About a third of the absorption systems do have redshifts higher than the emission redshift of QSOs, and thus appear to be infalling. The direct inference would be that lower  $\beta$  systems are closer to the ionization sources. No clues are found that distinguish the material as ambient material (shocked?) in the QSO host galaxies or as returning gas from QSO jet or accretion disk outflows.

8. The QSOs with nonzero radio flux in the FIRST survey are intrinsically redder than QSOs with null detection in the FIRST survey by relative  $E(B - V) \sim 0.04$ , on average, for an SMC extinction curve, even when there are no absorption lines present.

9. The incidence of associated Mg II systems with  $W_{\text{Mg}} > 0.3 \text{ \AA}$  in QSOs with nonzero FIRST radio flux is 1.7 times that in the QSOs with no detection in the FIRST survey.

10. Associated systems in QSOs with nonzero radio flux in the FIRST survey have 3–4 times as much dust as those in QSOs with null detection in the FIRST survey. This excess reddening is correlated with the strength of Mg II absorption lines and appears to originate in the absorbers themselves. These absorbers are thus significantly different from the intervening systems and may possibly be intrinsic to the QSOs.

11. No clear discriminant between associated and intervening systems has been found that would definitely work on a case-by-case basis, despite the clear but subtle differences in ionization and reddening noted above. “Intrinsic” but high ejection velocity systems may be hard to discern among the intervening systems, except through nondetection of a galaxy at the absorber redshift.

<sup>12</sup> An often mentioned criterion for a system being intrinsic is that it has variable absorption. In light of the recent realization that a number of “interstellar” lines in the Milky Way vary directly (Lauroesch & Meyer 2003; Welty 2007) and that there are very small scale structures that could cause variability owing to relative motion of the background source and subsequent sampling of different parts of a foreground interstellar cloud, there is evidently not yet one general technique that works in many individual cases.

D. V. B. and D. P. S. acknowledge the support from NSF grant AST06-07634. P. K. acknowledges support from the Department of Science and Technology (Government of India) grant SP/S2/HEP-07/03. D. G. Y. is grateful for support of students by the Kavli Institute. G. T. R. was supported in part by a Gordon and Betty Moore Fellowship in data intensive sciences at JHU. V. P. K. acknowledges support from NSF grant AST 06-07739 to the University of South Carolina.

Funding for the SDSS and SDSS-II has been provided by the Alfred P. Sloan Foundation, the Participating Institutions, the National Science Foundation, the US Department of Energy, the National Aeronautics and Space Administration, the Japanese Monbukagakusho, the Max Planck Society, and the Higher Education Funding Council for England. The SDSS Web Site is <http://www.sdss.org/>. The SDSS is managed by the Astrophys-

ical Research Consortium for the Participating Institutions. The Participating Institutions are the American Museum of Natural History, Astrophysical Institute Potsdam, University of Basel, University of Cambridge, Case Western Reserve University, University of Chicago, Drexel University, Fermilab, the Institute for Advanced Study, the Japan Participation Group, Johns Hopkins University, the Joint Institute for Nuclear Astrophysics, the Kavli Institute for Particle Astrophysics and Cosmology, the Korean Scientist Group, the Chinese Academy of Sciences (LAMOST), Los Alamos National Laboratory, the Max-Planck-Institute for Astronomy (MPIA), the Max-Planck-Institute for Astrophysics (MPA), New Mexico State University, Ohio State University, University of Pittsburgh, University of Portsmouth, Princeton University, the United States Naval Observatory, and the University of Washington.

## APPENDIX A

## THE ABSORBER AND MATCHING NONABSORBER SAMPLES

The list of absorbers in the full absorber sample (No. 1) and the corresponding best-matching nonabsorber sample is given in Table 5. The table lists plate, fiber, and MJD numbers,  $z_{\text{em}}$ ,  $\Delta(g-i)$ , and  $i$  magnitude for the absorber and the nonabsorber QSOs. Also listed are the  $z_{\text{abs}}$  and  $\beta$  values for the absorber sample. In Table 6 we give the absorber rest-frame equivalent widths, and their  $1\sigma$  errors, of Al II  $\lambda 1670$ , C IV  $\lambda \lambda 1548, 1550$ , Mg I  $\lambda 2852$ , Mg II  $\lambda \lambda 2796, 2803$ , Si IV  $\lambda \lambda 1396, 1403$ , and Fe II  $\lambda 2382$  for the absorption systems. The equivalent widths are in  $\text{\AA}$ . The full tables are available in the online *Journal*.

TABLE 5  
FULL ABSORBER AND MATCHING NONABSORBER SAMPLES

ABSORBER SAMPLE								NONABSORBER SAMPLE					
Plate	Fiber	MJD	$z_{\text{em}}$	$\Delta(g-i)$	$z_{\text{abs}}$	$i$ mag	$\beta$	Plate	Fiber	MJD	$z_{\text{em}}$	$\Delta(g-i)$	$i$ mag
0388.....	289	51793	1.2940	0.6225	1.2925	18.979	0.001	0760.....	124	52264	1.2920	-0.1023	18.978
0651.....	496	52141	1.3570	0.0484	1.3522	18.467	0.002	1044.....	455	52468	1.3610	0.2461	18.472
0390.....	418	51900	1.0130	0.7486	1.0134	18.843	0.000	1165.....	131	52703	1.0150	1.0350	18.844
0753.....	149	52233	1.7640	0.2852	1.7731	17.885	-0.003	0835.....	271	52326	1.7760	0.0737	17.801
0653.....	558	52145	1.8570	0.2630	1.8430	19.055	0.005	0583.....	469	52055	1.8510	1.3632	19.044
0753.....	034	52233	1.7080	0.1664	1.6870	18.100	0.008	0302.....	550	51688	1.7240	-0.0054	18.095
0392.....	528	51793	1.5400	0.3629	1.5498	18.687	-0.004	0763.....	117	52235	1.5370	0.1036	18.700
0392.....	189	51793	1.0660	0.0550	1.0500	18.741	0.008	0917.....	393	52400	1.0700	0.0108	18.751
0418.....	205	51817	1.2500	0.1302	1.2515	18.595	-0.001	0404.....	127	51812	1.2460	-0.0663	18.600
0655.....	389	52162	1.4720	-0.1273	1.4553	17.470	0.007	0448.....	433	51900	1.4750	0.1756	17.481
0655.....	239	52162	1.8810	0.0453	1.8566	18.393	0.009	0619.....	377	52056	1.8690	-0.0409	18.398
0655.....	536	52162	1.5250	0.0190	1.5230	18.952	0.001	0812.....	564	52352	1.5220	-0.1874	18.934
0655.....	177	52162	1.1630	0.0058	1.1425	18.467	0.010	1163.....	280	52669	1.1630	-0.0206	18.477
0419.....	056	51879	1.3840	-0.2027	1.3699	18.218	0.006	0634.....	471	52164	1.3780	-0.0937	18.219
0394.....	242	51913	1.5810	-0.0437	1.5559	18.774	0.010	1287.....	272	52728	1.5810	0.0727	18.764
0420.....	155	51871	1.7300	-0.0071	1.7027	18.162	0.010	0924.....	493	52409	1.7200	-0.0002	18.183
0658.....	527	52146	1.2720	-0.2076	1.2754	18.928	-0.001	0751.....	286	52251	1.2720	-0.1203	18.934
0397.....	267	51794	1.3730	0.1363	1.3710	17.248	0.001	1332.....	519	52781	1.3710	-0.0953	17.200
0660.....	190	52177	1.6920	-0.0260	1.7007	17.914	-0.003	1350.....	297	52786	1.6990	-0.1325	17.850
0398.....	110	51789	1.4970	0.4441	1.4864	18.088	0.004	0520.....	024	52288	1.4990	0.0729	18.059
0661.....	362	52163	1.8360	0.0305	1.8078	17.151	0.010	0326.....	292	52375	1.7700	0.0479	17.108
0425.....	447	51898	1.3040	0.6804	1.2921	18.830	0.005	0749.....	432	52226	1.3090	0.3725	18.822
0662.....	565	52147	1.8390	-0.0588	1.8181	18.987	0.007	1171.....	305	52753	1.8400	-0.0192	18.992
0401.....	255	51788	1.6590	-0.1123	1.6746	17.495	-0.006	1209.....	555	52674	1.6640	-0.1576	17.405
0429.....	328	51820	1.7590	-0.0165	1.7909	18.186	-0.011	0345.....	128	51690	1.7440	0.0256	18.193
0430.....	362	51877	1.7380	0.4237	1.7385	19.918	0.000	0453.....	195	51915	1.7350	0.0215	19.912
0427.....	402	51900	1.7000	0.0348	1.7085	17.618	-0.003	0448.....	172	51900	1.7070	-0.0999	17.595
0404.....	070	51812	1.5200	0.0978	1.5053	19.077	0.006	0516.....	108	52017	1.5190	-0.1447	19.070
0667.....	220	52163	1.7340	0.4091	1.7205	18.902	0.005	1044.....	230	52468	1.7300	-0.1700	18.929
0405.....	073	51816	1.5570	-0.1534	1.5838	18.089	-0.010	0523.....	062	52026	1.5540	0.0543	18.047
0454.....	064	51908	1.2540	0.3680	1.2565	18.946	-0.001	0761.....	096	52266	1.2520	-0.0956	18.942
0455.....	638	51909	1.2200	-0.1423	1.2134	19.833	0.003	0648.....	238	52559	1.2150	0.7185	19.830
0410.....	318	51816	1.4600	-0.0996	1.4344	17.738	0.010	0540.....	568	51996	1.4650	0.1462	17.772
0457.....	354	51901	1.4560	-0.0627	1.4330	18.178	0.009	0590.....	282	52057	1.4510	0.3246	18.178

NOTE.—Table 5 is published in its entirety in the electronic edition of the *Astrophysical Journal*. A portion is shown here for guidance regarding its form and content.

TABLE 6  
EQUIVALENT WIDTHS OF CHOSEN LINES

PLATE	FIBER	MJD	REST EQUIVALENT WIDTHS (Å)									
			Al II $\lambda$ 1670	C IV $\lambda$ 1548	C IV $\lambda$ 1550	Mg I $\lambda$ 2852	Mg II $\lambda$ 2796	Mg II $\lambda$ 2803	Si IV $\lambda$ 1393	Si IV $\lambda$ 1403	Fe II $\lambda$ 2382	
0388.....	289	51793	-1.00, 0.34	-1.00, -1.00	-1.00, -1.00	0.68, 0.11	0.57, 0.09	0.56, 0.08	-1.00, -1.00	-1.00, -1.00	-1.00, 0.17	
0651.....	496	52141	0.52, 0.12	-1.00, -1.00	-1.00, -1.00	-1.00, 0.20	0.98, 0.06	0.78, 0.05	-1.00, -1.00	-1.00, -1.00	0.62, 0.08	
0390.....	418	51900	-1.00, -1.00	-1.00, -1.00	-1.00, -1.00	-1.00, 0.15	0.80, 0.09	0.70, 0.08	-1.00, -1.00	-1.00, -1.00	0.38, 0.12	
0753.....	149	52233	1.23, 0.10	2.10, 0.10	1.27, 0.09	0.44, 0.12	2.60, 0.10	2.45, 0.08	1.00, 0.14	1.12, 0.15	1.44, 0.08	
0653.....	558	52145	0.98, 0.16	1.61, 0.11	1.02, 0.09	-1.00, 0.27	2.77, 0.20	1.51, 0.17	0.76, 0.16	-1.00, 0.25	0.95, 0.12	
0753.....	034	52233	-1.00, 0.08	0.36, 0.06	0.19, 0.06	-1.00, 0.16	0.87, 0.09	0.54, 0.07	-1.00, -1.00	-1.00, -1.00	0.47, 0.06	
0392.....	528	51793	0.93, 0.22	1.24, 0.20	1.11, 0.22	0.74, 0.11	1.96, 0.07	1.60, 0.07	-1.00, -1.00	-1.00, -1.00	1.23, 0.13	
0392.....	189	51793	-1.00, -1.00	-1.00, -1.00	-1.00, -1.00	-1.00, 0.23	2.32, 0.16	2.00, 0.14	-1.00, -1.00	-1.00, -1.00	1.20, 0.11	
0418.....	205	51817	-1.00, -1.00	-1.00, -1.00	-1.00, -1.00	0.70, 0.10	1.58, 0.08	1.78, 0.09	-1.00, -1.00	-1.00, -1.00	1.27, 0.08	
0655.....	389	52162	0.46, 0.04	-1.00, -1.00	-1.00, -1.00	0.16, 0.03	1.05, 0.04	0.92, 0.03	-1.00, -1.00	-1.00, -1.00	0.42, 0.04	
0655.....	239	52162	0.48, 0.08	0.36, 0.06	0.16, 0.04	-1.00, 0.18	1.23, 0.11	1.06, 0.10	-1.00, 0.09	0.46, 0.10	0.74, 0.07	
0655.....	536	52162	0.82, 0.20	1.36, 0.10	1.36, 0.11	0.41, 0.07	1.72, 0.07	1.25, 0.07	-1.00, -1.00	-1.00, -1.00	1.13, 0.13	
0655.....	177	52162	-1.00, -1.00	-1.00, -1.00	-1.00, -1.00	0.19, 0.05	1.46, 0.08	1.06, 0.07	-1.00, -1.00	-1.00, -1.00	0.39, 0.06	
0419.....	056	51879	0.42, 0.12	-1.00, -1.00	-1.00, -1.00	0.43, 0.10	1.60, 0.06	1.51, 0.06	-1.00, -1.00	-1.00, -1.00	0.90, 0.08	
0394.....	242	51913	0.70, 0.12	-1.00, 0.11	-1.00, 0.11	0.42, 0.05	1.37, 0.08	1.10, 0.08	-1.00, -1.00	-1.00, -1.00	0.63, 0.07	
0420.....	155	51871	0.18, 0.05	0.62, 0.05	0.50, 0.04	0.55, 0.13	0.53, 0.06	0.64, 0.09	-1.00, -1.00	-1.00, -1.00	-1.00, 0.06	
0658.....	527	52146	-1.00, -1.00	-1.00, -1.00	-1.00, -1.00	0.96, 0.18	2.25, 0.15	2.30, 0.11	-1.00, -1.00	-1.00, -1.00	1.84, 0.25	
0397.....	267	51794	0.42, 0.06	-1.00, -1.00	-1.00, -1.00	0.22, 0.03	0.55, 0.03	0.49, 0.03	-1.00, -1.00	-1.00, -1.00	0.42, 0.04	
0660.....	190	52177	0.31, 0.07	1.92, 0.07	0.68, 0.05	0.40, 0.08	0.82, 0.06	0.81, 0.05	-1.00, -1.00	-1.00, -1.00	-1.00, 0.06	
0398.....	110	51789	-1.00, 0.10	1.37, 0.14	2.63, 0.44	-1.00, 0.14	0.44, 0.06	0.38, 0.06	-1.00, -1.00	-1.00, -1.00	-1.00, 0.08	
0661.....	362	52163	-1.00, 0.04	0.61, 0.04	0.51, 0.03	0.26, 0.07	0.42, 0.07	0.36, 0.05	0.40, 0.08	0.23, 0.05	-1.00, 0.04	
0425.....	447	51898	0.69, 0.03	-1.00, -1.00	-1.00, -1.00	0.67, 0.09	1.73, 0.08	1.68, 0.07	-1.00, -1.00	-1.00, -1.00	0.94, 0.28	
0662.....	565	52147	0.63, 0.14	-1.00, 0.12	0.40, 0.10	-1.00, 0.33	1.64, 0.21	2.09, 0.20	0.60, 0.15	-1.00, 0.21	1.30, 0.12	

NOTE.—In cols. (4)–(12), the first number is the equivalent width, while the second number is the  $1\sigma$  error, in Å, in the absorber rest frame; -1.0 for the equivalent width indicates that the line was not detected, while -1.0 for the error means that the line was not covered by the SDSS spectrum. Table 6 is published in its entirety in the electronic edition of the *Astrophysical Journal*. A portion is shown here for guidance regarding its form and content.

## REFERENCES

- Adelman-McCarthy, J., et al. 2007, *ApJS*, 172, 634  
Aldcroft, T. L., Bechtold, J., & Elvis, M. 1994, *ApJS*, 93, 1  
Anderson, S. F., Weymann, R. J., Foltz, C. B., & Chaffee, F. H. 1987, *AJ*, 94, 278  
Anderson, S. F., et al. 2007, *AJ*, 133, 313  
Arav, N., Li, Z.-Y., & Begelman, M. C. 1994, *ApJ*, 432, 62  
Baker, J. C., Hunstead, R. W., Athreya, R. M., Barthel, P. D., de Silva, E., Lehnert, M. D., & Suaners, R. D. E. 2002, *ApJ*, 568, 592  
Baldwin, J. A., Hamann, F., Korista, K. T., Ferland, G. J., Dietrich, M., & Warner, C. 2003, *ApJ*, 583, 649  
Barlow, T. A., & Sargent, W. L. W. 1997, *AJ*, 113, 136  
Becker, R., White, R., & Helfand, D. 1995, *ApJ*, 450, 559  
Blanton, M. R., Lupton, R. H., Maley, F. M., Young, N., Zehavi, I., & Loveday, J. 2003, *AJ*, 125, 2276  
Bowen, D. V., et al. 2006, *ApJ*, 645, L105  
Brotherton, M. S., et al. 2001, *ApJ*, 546, 775  
Burbidge, E. M., Lynds, C. R., & Burbidge, G. R., *ApJ*, 1966, 144, 447  
Chelouche, D., Menard, B., Bowen, D. V., & Gnat, O. 2007, *ApJ*, submitted (arXiv: 0706.4336)  
Chelouche, D., & Netzer, H. 2005, *ApJ*, 625, 95  
Christensen, L., Jahnke, K., Wisotzki, L., & Sanchez, S. F. 2006, *A&A*, 459, 717  
Churchill, C. W., Rigby, J. R., Charlton, J. C., & Voigt, S. S. 1999, *ApJS*, 120, 51  
Crawford, C. S., & Fabian, A. C. 1989, *MNRAS*, 239, 219  
Dhanda, N., Baldwin, J. A., Bentz, M. C., & Osmer, P. S. 2007, *ApJ*, 658, 804  
D'Odorico, V. 2007, *A&A*, 470, 523  
D'Odorico, V., Cristiani, S., Romano, D., Granato, G. L., & Danese, L. 2004, *MNRAS*, 351, 976  
Everett, J. E. 2005, *ApJ*, 631, 689  
Feigelson, E. D., & Nelson, P. I. 1985, *ApJ*, 293, 192  
Ferland, G. J., Baldwin, J. A., Korista, K. T., Hamann, R., Carswell, R. F., Phillips, M., Wilkes, B., & Williams, R. E. 1996, *ApJ*, 461, 683  
Fitzpatrick, E. L. 1999, *PASP*, 111, 63  
Foltz, C. B., Chaffee, F. H. Jr., Weyman, R. J., Anderson, S. F. 1988, in *QSO Absorption Lines: Probing the Universe*, ed. J. C. Blades, D. A. Turnshek, & C. A. Norman (Cambridge: Cambridge Univ. Press), 53  
Foltz, C. B., Weyman, R. J., Peterson, B. M., Sun, L., Malkan, M. A., & Chaffee, F. H. 1986, *ApJ*, 307, 504  
Fu, H., & Stockton, A. 2006, *ApJ*, 650, 80  
———. 2007a, *ApJ*, 666, 794  
———. 2007b, *ApJ*, 664, L75  
Fukugita, M., & Peebles, P. J. E. 2006, *ApJ*, 639, 590  
Fukugita, M., et al. 1996, *AJ*, 111, 1748  
Ganguly, R., Bond, N. A., Charlton, J. C., Eracleous, M., Brandt, W. N., & Churchill, C. W. 2001, *ApJ*, 549, 133  
Garnett, D. R., Shields, G. A., Peimbert, M., Torres-Peimbert, S. Skillman, E. D., Dufour, R. J., Terlevich, E., & Terlevich, R. J. 1999, *ApJ*, 513, 168  
Gaskell, C. M. 1982, *ApJ*, 263, 79  
Groves, B. A., Heckman, T. M., & Kaufmann, G. 2006, *MNRAS*, 371, 1559  
Gunn, J. E., et al. 1998, *AJ*, 116, 3040  
———. 2006, *AJ*, 131, 2332  
Haiman, Z., & Rees, M. J. 2001, *ApJ*, 556, 87  
Hamann, F. 1997, *ApJS*, 109, 279  
Hamann, F. W., Barlow, T. A., Chaffee, F. C., Foltz, C. B., & Weymann, R. J. 2001, *ApJ*, 550, 142  
Hamann, F., Barlow, T. A., & Junkkarinen, V. T. 1997a, *ApJ*, 478, 87  
Hamann, F., Barlow, T. A., Junkkarinen, V., & Burbidge, E. M. 1997b, *ApJ*, 478, 80  
Hamann, F., & Ferland, G. 1999, *ARA&A*, 37, 487  
Hamann, F., Korista, K. T., Ferland, G. J., Warner, C., & Baldwin, J. 2002, *ApJ*, 564, 592  
Heckman, T. M., Armus, L., & Miley, G. K. 1990, *ApJS*, 74, 833  
Heckman, T. M., Dahlem, M., Eales, S. A., Babbiano, G., & Weaver, K. 1996, *ApJ*, 457, 616  
Heckman, T. M., Lehnert, M. D., Strickland, D. K., & Armus, L. 2000, *ApJS*, 129, 493  
Heckman, T. M., Miley, G. K., Lehnert, M. D., & van Breugel, W. 1991, *ApJ*, 370, 78  
Hogg, D. W., Finkbeiner, D. P., Schlegel, D. J., & Gunn, J. E. 2001, *AJ*, 122, 2129  
Ivezić, Ž., et al. 2002, *AJ*, 124, 2364  
———. 2004, *Astron. Nachr.*, 325, 583  
Jahnke, K., Kuhlbrodt, B., & Wisotzki, L. 2004, *MNRAS*, 352, 399  
Januzzi, B. T., et al. 1996, *ApJ*, 470, L11  
Junkkarinen, V. T., Cohen, R. D., Beaver, E. A., Burbidge, E. M., Lyons, R. W., & Madjewski, G. 2004, *ApJ*, 614, 658

- Khare, P., Kulkarni, V. P., Lauroesch, J. T., York, D. G., Crotts, A. P. S., & Nakamura, O. 2004, *ApJ*, 616, 86
- Konigl, A., & Kartje, J. F. 1994, *ApJ*, 434, 446
- Krolik, J. H., & Kriss, G. A. 2001, *ApJ*, 561, 684
- Lauroesch, J. T., & Meyer, D. M. 2003, *ApJ*, 591, L123
- Letawe, G., Magain, P., Courbin, F., Jablonka, P., Jahnke, K., Meylan, G., & Wisotzki, L. 2007, *MNRAS*, 378, 83
- McCarthy, P. 1993, *ARA&A*, 31, 639
- Mediavilla, E., Munoz, J. A., Kochanek, C. S., Falco, E. E., Arribas, S., & Motta, V. 2005, *ApJ*, 619, 749
- Meiring, J. D., et al. 2006, *MNRAS*, 370, 43
- Meiring, J. D. 2007, *MNRAS*, 376, 557
- Miller, L., Peacock, J. A., & Mead, A. R. G. 1990, *MNRAS*, 244, 207
- Misawa, T., Charlton, J. C., Racleous, M., Ganguly, R., Tytler, D., Kirkman, D., Suzuki, N., & Lubin, D. 2007, *ApJS*, 171, 1
- Motta, V., et al. 2002, *ApJ*, 574, 719
- Murray, N., Chang, J., Grossman, S. A., & Voit, G. M. 1995, *ApJ*, 451, 498
- Nagao, T., Marconi, A., & Maiolino, R. 2006, *A&A*, 447, 157
- Orr, M. J. L., & Browne, I. W. A. 1982, *MNRAS*, 200, 1067
- Padovani, P., & Urry, C. M. 1992, *ApJ*, 387, 449
- Pereyra, N. A., Vanden Berk, D. E., Turnshek, D. A., Hillier, D. J., Wilhite, B. C., Kron, R. G., Schneider, D. P., & Brinkmann, J. 2006, *ApJ*, 642, 87
- Peroux, C., Kulkarni, V. P., Meiring, J., Ferlet, R., Khare, P., Lauroesch, J. T., Vladilo, G., & York, D. G. 2006, *A&A*, 450, 53
- Petitjean, P., Rauch, M., & Carswell, R. F. 1994, *A&A*, 291, 29
- Pier, J., Munn, J. A., Hindsley, R. B., Hennessy, G. S., Kent, S. M., Lupton, R. H., & Ivezić, 2003, *AJ*, 125, 1559
- Proga, D., Stone, J. M., & Kallman, T. R. 2000, *ApJ*, 543, 686
- Rao, S. M., & Turnshek, D. A. 2000, *ApJS*, 130, 1
- Richards, G. T. 2006, preprint (astro-ph/0603827)
- . 2001, *ApJS*, 133, 53
- Richards, G. T., Laurent-Muehleisen, S. A., Becker, R. H., & York, D. G. 2001, *ApJ*, 547, 635
- Richards, G. T., York, D. G., Yanny, B., Kollgaard, R. L., Laurent-Muehleisen, S. A., & Vanden Berk, D. E. 1999, *ApJ*, 513, 576
- Richards, G. T., et al. 2002a, *AJ*, 123, 2945
- . 2002b, *AJ*, 124, 1
- . 2003, *AJ*, 126, 1131
- Sargent, W. L. W., Boksenberg, A., & Steidel, C. C. 1988, *ApJS*, 68, 539
- Schlegel, D. J., Finkbeiner, D. P., & Davis, M. 1998, *ApJ*, 500, 525
- Schneider, D. P., et al. 2005, *AJ*, 130, 367
- . 2007, *AJ*, 134, 102
- Serber, W., Bahcall, N., Menard, B., & Richards, G. T. 2006, *ApJ*, 643, 68
- Smith, J. A., et al. 2002, *AJ*, 123, 2121
- Steidel, C. C., Dickinson, M., Meyer, D. M., Adelberger, K. L., & Sembach, K. R. 1997, *ApJ*, 480, 568
- Stockton, A. N., & Lynds, C. R. 1966, *ApJ*, 144, 451
- Stoughton, C., et al. 2002, *AJ*, 123, 485
- SubbaRao, M., Frieman, J., Bernardi, M., Loveday, J., Nichol, B., Castander, F., & Meiksin, A. 2002, *Proc. SPIE*, 4847, 452
- Tripp, T. M., Lu, L., & Savage, B. D. 1996, *ApJS*, 102, 239
- Trump, J. R., et al. 2006, *ApJS*, 165, 1
- Tucker, D., et al. 2006, *Astron. Nachr.*, 327, 821
- Tytler, D., & Fan, X. 1992, *ApJS*, 79, 1
- Vanden Berk, D. E., Quashnock, J. M., York, D. G., & Yanny, B. 1996, *ApJ*, 469, 78
- Vanden Berk, D. E., et al. 2001, *AJ*, 122, 549
- . 2005, *AJ*, 129, 2047
- Vestergaard, M. 2003, *ApJ*, 599, 116 (V03)
- Voges, W., et al. 1999, *A&A*, 349, 389
- Wake, D. A., et al. 2004, *ApJ*, 610, L85
- Wampler, E. J., Chugai, N. N., & Petitjean, P. 1995, *ApJ*, 443, 586
- Wang, J., Hall, P. B., Ge, J., Li, A., & Schneider, D. P. 2004, *ApJ*, 609, 589
- Welty, D. 2007, *ApJ*, 668, 1012
- Weymann, R. J., Williams, R. E., Peterson, B. M., & Turnshek, D. A. 1979, *ApJ*, 234, 33
- White, R. L., & Becker, R. H. 1992, *ApJS*, 79, 331
- Wilkes, B. J. 1984, *MNRAS*, 207, 73
- Yip, C. W., et al. 2004, *AJ*, 128, 2603
- York, D. G., & Kinahan, B. 1979, *ApJ*, 228, 127
- York, D. G., et al. 2000, *AJ*, 120, 1579
- . 2005, in *IAU Colloq. 199, Probing Galaxies through Quasar Absorption Lines*, ed. P. R. Williams, C.-G. Shu, & B. Menard, (Cambridge: Cambridge Univ. Press), 58
- . 2006, *MNRAS*, 367, 945 (Y06)
- Young, P., Sargent, W. L. W., & Boksenberg, A. 1982, *ApJS*, 48, 455